augustus 1977

›r Cultuurtechniek en Waterhuishouding
Wageningen

ON YIELD FUNCTIONS IN SOIL MECHANICS, SOIL TESTING METHODS AND SHEAR STRENGTH OF SOILS

ir. J. Bakker

C O N T E N T S

1. INTRODUCTION

1.1. The need of soil mechanics in agriculture

The need of soil mechanics in agriculture is encountered in problems such as compaction of the soil by agricultural machinery, execution of drainage works, workability of the soil, traction performance of agricultural machines, bearing capacity of soils, condition of sport fields on different soils and under varying moisture conditions.

In all these examples there are forces acting on the soil which give rise to stresses and strains in the soil. In agriculture one is interested in this stress-strain relationship in order to predict the compaction of the soil after a certain activity in which the soil has been exposed to forces produced by the wheight of heavy machinery. For the evalution of traction performance one must know the maximum shear strength of the soil.

There are different theories to describe the soil behaviour under compression and or tension. We will treat several of these theories which are called failure theories from which the Coulomb-Mohr failure law is most commonly used (chapter 2).

The soil parameters such as shear strength and stress-strain relationship etc. can be measured with several different test devices. The different test devices do not always give the same values for the soil parameters under investigation. Here an effort is made to give an evaluation of these methods (chapter 3).

We will also indicate the most accurate test to investigate a certain soil mechanical problem in agricultural engineering. The best

procedure to estimate the strength, compactibility etc. of the soil is to run tests that duplicate the field conditions as closely as possible, same degree of saturation, same total stress, and if possible the same pressure in the liquid phase.

Because the values for the soil parameters of most common agricultural soils are not readily available in literature it was found useful to collect these data and to indicate the influence of soil density, moisture content and clay content on these parameters.

As the Coulomb-Mohr failure theory is used most widely at present we give the value of c and ϕ , the analytical cohesion and friction angle respectively, and the shear strength for the most common soils under different moisture and compaction conditions. These values have been found in literature and were obtained with different test procedures and sometimes not specified failure criteria and moisture and density conditions (chapters 4 and 5). The accuracy of the values is $\pm$ 25% and one should use the values for preliminary calculations only.

2. YIELD CRITERIA AND FAILURE THEORIES

2.1. The concepts of yield and failure in soils

The terms yield and failure cannot be applied indiscriminately to soils. The failure of brittle materials, such as cast iron on rock, occurs as a fracture with little or no plastic yielding. This fracture can be readily identified with failure.

The term 'yield' in the field of plasticity is used to describe the onset of plastic deformation, or, conversely, the upper limit of elastic action (see fig. 2.1.).

The precise definition of yield in an actual material is related to the characteristics of the stress-strain curve of the material; only when there is a sharp break between the elastic portion (recoverable deformation) and the plastic portion (non-recoverable deformation) of the stress-strain curve yield can be accurately defined.

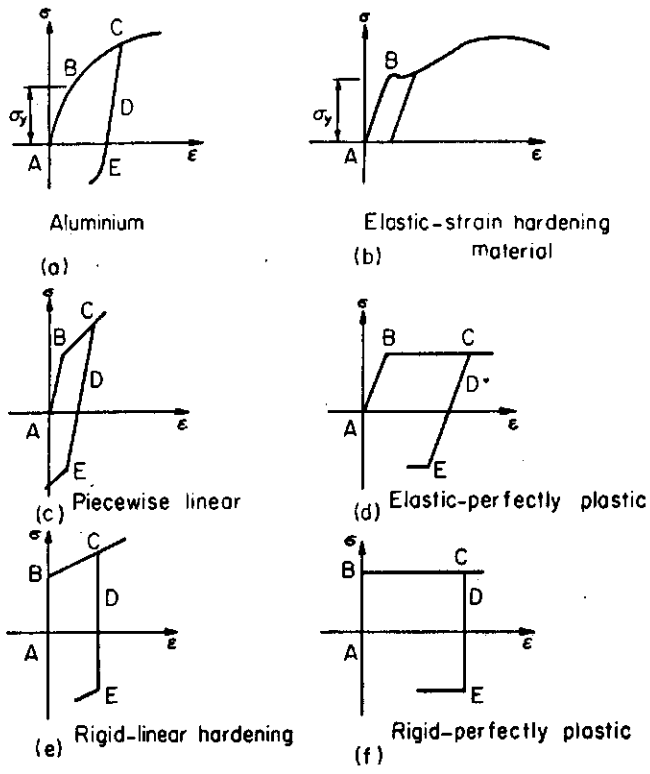

Fig. 2.1. Typical stress-strain curves for various kinds of materials. The yield stress σ_y occurs at point B in a-f. From YONG (1975)

In the fig. 2.1. a perfectly plastic material exhibits a continued strain performance at the yield stress if the stress is sustained, as in fig. 2.1. d and f. The term plastic strain which is commonly used denotes irrecoverable strain performance as in curve BC in fig. 2.1. a. In this case, strain hardening is shown by BC. The term fracture implies the appearance of distinct surfaces of separations in the body, whereas yield is used to describe the onset of plastic deformation with the resulting unrestricted plastic deformation defined as flow. 'Failure' in a general sense includes both fracture and flow. The curve DE shows what happens when the compressive load is withdrawn and replaced by a tensile force.

2.2. Principal stress space

A convenient way to examine the state of stress producing yield on failure in a material specimen is to plot the principal stress components σ1, σ2 and σ3 at yield or failure in principal stress space (fig. 2.2.).

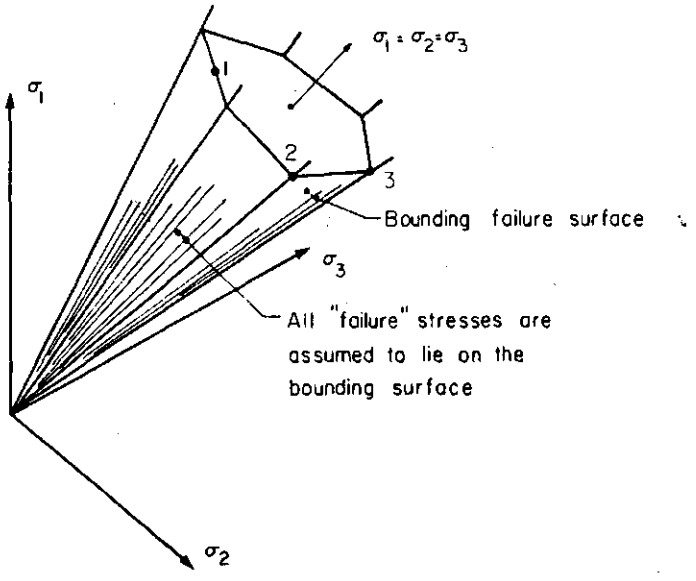

Fig. 2.2. Principal-stress space showing principal stresses at time of failure (or yielding). Diagram shows the Mohr-Coulomb failure surface as an example. From YONG (1975)

Point 1 in fig. 2.2. represents a σ1, σ2 and σ3 combination producing yield in a material in a particular stressing situation. Similarly point 2 represents another σ1, σ2 and σ3 principal stress combination obtained at yield for another stressing situation. By applying various stress situations the line joining the points are a common octahedral plane (i.e. ¶ plane) will define a surface which is called the yield surface. The function f (σ1, σ2, σ3) is thus called the yield function.

If points 1, 2 and 3 represent stress situations at failure, the surface defined is termed a failure surface and the function f (σ1, σ2, σ3) will be called a failure function or failure theory. This will be examined in detail in a later section.

2.2.1. Various types of modules in stress-strain relationship

Concepts from the theory of elasticity

If we apply an uniaxial stress σz to an elastic cylinder (fig. 2.3.) there will be a vertical compression and a lateral expansion such that,

$$\varepsilon z = \frac{\sigma z}{E} \quad (1) \qquad \varepsilon_x = \varepsilon_y = -\mu\varepsilon_z \quad (2)$$

where

ε_x, ε_y, ε_z = strains in the x, y, z directions, respectively

E = Young's modules of elasticity

μ = Poisson's ratio

If shear stress τzx are applied to an elastic cube, there will be a shear distortion such that

$$fzx = \frac{\tau zx}{G} \quad (3)$$

where three G = shear modules. Equations 1 to 3 define the three basic constants of the theory of elasticity: E, G and μ.

Actually only two of these constants are needed since

$$G = \frac{E}{2(1+\mu)} \quad (4)$$

For an elastic material with all stress components acting, we can employ the principle of superposition to obtain:

$$ex = \frac{1}{E}\left\{\sigma x - \mu\,(\sigma y+\sigma z)\right\} \quad (5a)$$

$$ey = \frac{1}{E}\left\{\sigma y - \mu\,(\sigma z+\sigma x)\right\} \quad (5b)$$

$$ez = \frac{1}{E}\left\{\sigma z - \mu\,(\sigma x+\sigma y)\right\} \quad (5c)$$

$$fxy = \frac{\tau xy}{G} \quad (5d)$$

$$fyz = \frac{\tau yz}{G} \quad (5e)$$

$$fzx = \frac{\tau zx}{G} \quad (5f)$$

the volumetric strain is

$$\frac{\Delta V}{V} = ex + ex + ez \quad (5g)$$

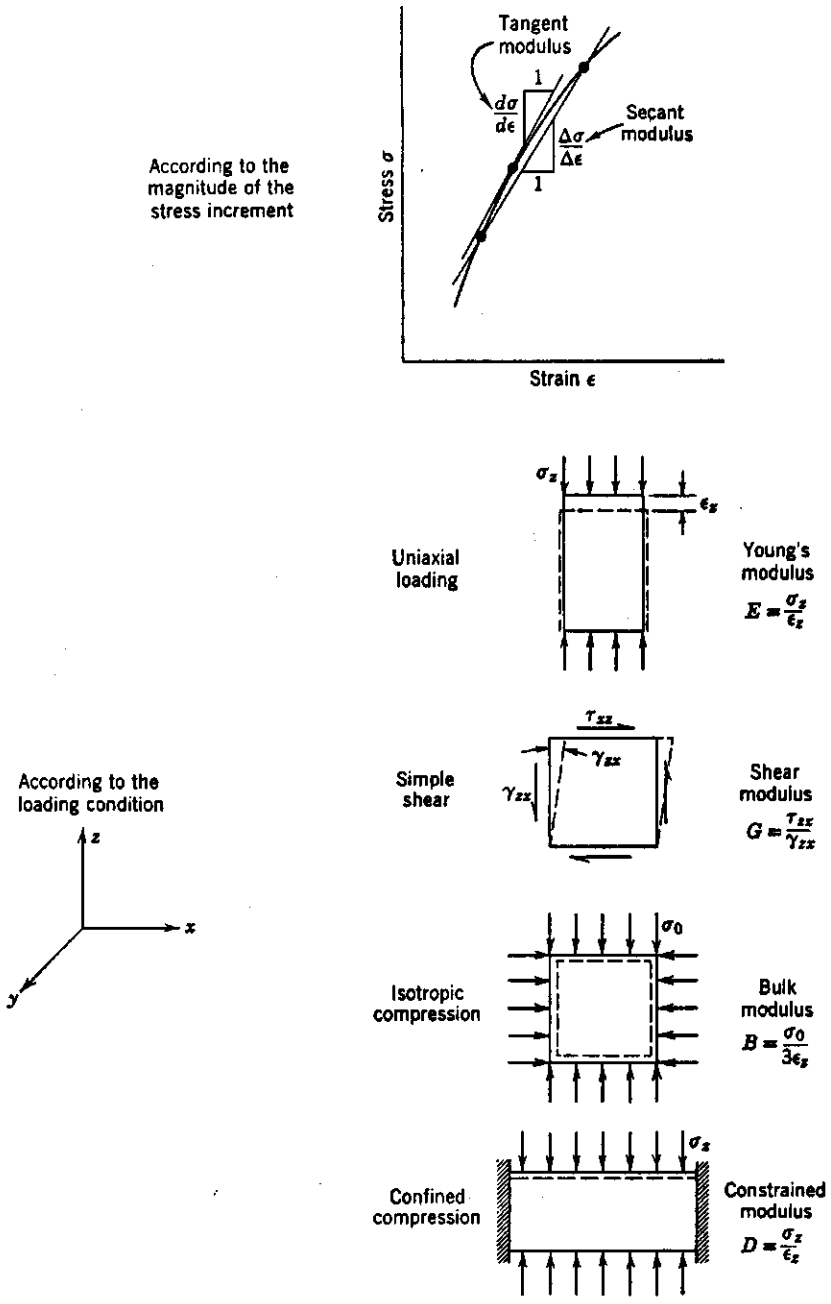

Fig. 2.3. Various types of modulus

For the special case where $\sigma x=\sigma y=\sigma z=\sigma o$ and $\tau xy=\tau yz=\tau zx=o$ the volume change equals

$$\frac{\Delta V}{V} = \frac{3\sigma o}{E}(1-2\mu)$$

The bulk modulus B is defined as

$$B = \frac{\sigma o}{\Delta V/V} = \frac{E}{3(1-2\mu)} \tag{6}$$

Still another special type of modulus is the constrained modulus D which is the ratio of axial stress to axial strain for confined compression. This modulus can be computed from eq. (5) by setting $\epsilon x=\epsilon y=o$.

Thus

$$\sigma x = \sigma y = \frac{\mu}{1-\mu}\sigma z \tag{7}$$

$$D = \frac{E(1-\mu)}{(1+\mu)(1-2\mu)} \tag{8}$$

Uniaxial loading and confined compression involve both shear strain and volume change.

2.3. Yield Criteria

2.3.1. The maximum-stress theory

The oldest theory of yielding and failure, sometimes known as Rankine's theory, postulates that the maximum principal stress in the material determines failure regardless of the magnitudes and senses of the other two principal stresses. This gives rise to its name "maximum-stress theory". Thus yielding in a stressed body in accordance with this theory begins when the absolute value of the maximum stress reaches the yield point stress of the material in simple tension or compression.

Plotted in principal stress space the yield surface representing this theory is a cube as shown in the projected view of principal stress space (on to the $\sigma 1$, $\sigma 2$ axes) in fig. 2.4.

The theory is contradicted in solid materials where three equal tensile or compressive stresses cannot produce a plastic but only an elastic deformation.

For those materials in which hydrostatic compressive stresses do

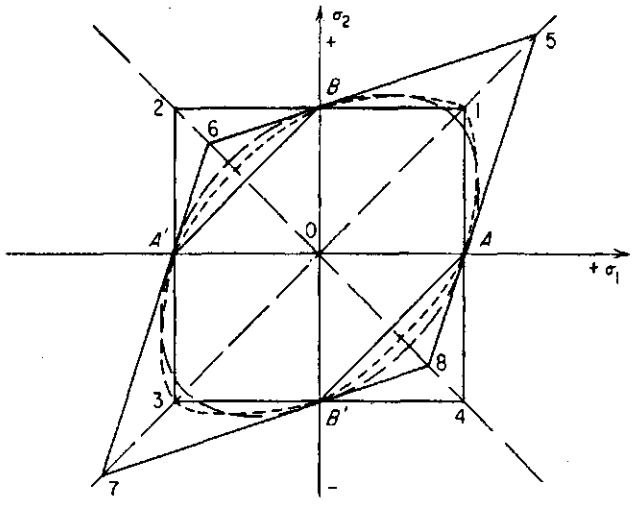

1234 = Maximum-stress theory
5678 = Maximum-strain theory
AIBA'3B'A = Maximum-shear theory
—— —— = Maximum-strain-energy theory
- - - - - - = Maximum-distortional-energy theory
Material assumed to have same yield point in tension and compression

Fig. 2.4. Representation of maximum shear-stress equation. (Timoshenko, 1956, published by Van Nostrand-Reinhold Co., 1955 Litton Educational Publ. Inc.) from Yong, 1975

cause plastic deformation, the theory is contradited by the fact that failure in simple tension in an isotropic material would be along inclined planes on which neither the tensile nor compressive stress is a maximum.

However, there is some merit in the theory when one considers the strength of non-isotropic materials, particularly layered materials, where there is a pronounced difference in strength properties in different directions, e.g., a layered rock might have almost no tensile strength in the direction normal to the layers and would fail in tension by splitting along these layers.

The theory has also found some use in a modified form to explain the cleavage fracture of crystals.

With these few exceptions the theory finds no application in modern practice.

2.3.2. The maximum elastic-strain theory

The maximum elastic-strain theory, attributed to St. Venant, assumes that a ductile material begins to yield when either the maximum (elongation) strain equals the yield point strain in simple tension, i.e.

$$\frac{\sigma 1}{E} - \frac{\mu}{E}(\sigma 2+\sigma 3) = \frac{\sigma y \text{ (tensile)}}{E} \qquad (2.1.)$$

or the minimum (shortening) strain equals the yield point strain in simple compression,

$$\left|\frac{\sigma 3}{E} - \frac{\mu}{E}(\sigma 1+\sigma 2)\right| = \frac{\sigma y \text{ (compressive)}}{E} \qquad (2.2.)$$

where the principal stresses $\sigma 1$, $\sigma 2$ and $\sigma 3$ are considered positive in tension, and are ordered such that $\sigma 1>\sigma 2>\sigma 3$ and μ, E and σy are Poisson's ratio, Young's modulus and yield point stress respectively.

In principal stress space the yield surface corresponding to theory consists of two straight three-sided pyramids in inverted positions relative to each other, having equilateral triangles as sections normal to the axis which coincides with one of the space diagonals, e.g. $\sigma 1=\sigma 2=\sigma 3$ (see fig. 2.4.)

The slopes of the sides of the pyramids would depend on Poisson's ratio. This theory is again contradicted by material behaviour under hydrostatic tensile or compressive stresses.

2.3.3. The constant elastic-strain energy theory

The quantity of strain energy per unit volume of the material is used as the basis for determining failure in the constant elastic-strain-energy theory. If we equate the strain energy for a given state of stress at failure to the energy stored at yield in simple tension the criterion may be written as:

$$\frac{(\sigma y)^2}{2E} = \frac{1}{2E}(\sigma 1^2+\sigma 2^2+\sigma 3^2) - \frac{\mu}{E}(\sigma 1\sigma 2+\sigma 2\sigma 3+\sigma 3\sigma 1) \qquad (2.3.)$$

Again, the performance of materials under hydrostatic stresses indicates that the elastic energy can have no significance as a limiting condition.

2.3.4. The maximum shear-stress theory

The maximum shear-stress theory assumes that yielding begins when the maximum shear stress in the material equals the maximum shear stress at the yield point in simple tension.

The maximum shear stress in a material under some general state of stress ($\sigma1>\sigma2>\sigma3$) is $(\sigma1-\sigma3)/2$ and the maximum shear stress in a tension test is equal to half the normal stress, $\sigma y/2$. The condition for yielding is thus given as:

$$(\sigma1-\sigma3) = \sigma y \qquad (2.4.)$$

This theory was advanced by Tresca in the period 1865 to 1870 and is generally attributed to him. It is a direct consequence of the Coulomb theory for a frictionless material. The maximum shear-stress theory (Coulomb theory) has been extended by Navier to account for pressures normal to the failure plane, which leads to its reference as the Coulomb-Navier theory.

The concept of maximum shear stress to explain a fracture type failure in a cohesive soil appears in the work of Collin (1846).

Tresca's contribution to this theory appears to account for a yielding type of failure. The results shown by Guest (1900) supported this criterion and the theory which is thus sometimes referred to as Guest's Law.

In its most useful form the theory may be stated as follows:

$$\tau max = \frac{\sigma1-\sigma3}{2} = \text{constant} \qquad (2.5.)$$

In uniaxial tension, $\sigma1=\sigma0$, $\sigma2=\sigma3=0$ and $\tau max=\sigma0/2$. In uniaxial compression, $\sigma1=\sigma2=0$, $\sigma3=-\sigma0$. Thus $\tau max=-(\sigma0/2)$.

Hence the yield condition requires that:

$$\tau max = \frac{1}{2}(\sigma1-\sigma3) = \frac{\sigma0}{2} \qquad (2.6.)$$

Eg. 2.6. requires that the yield stress of the material in either simple tension or compression must be equal, which is approximately true in the case of mild steel.

The "slip lines" (failure lines on planes) which appear at the onset of plastic flow should be inclined at an angle of 45^{o} with respect to the directions of the principal stress $\sigma1$ and $\sigma3$, that is,

coincident with the directions of maximum shearing stress.

The condition of flow does not contain the intermediate principal stress, σ2, which can have any value between σ1 and σ3.

The flow condition in its most general form may be expressed by three equations:

$$\sigma 1-\sigma 3 = \pm\sigma y;\ \sigma 2-\sigma 1 = \pm\sigma y;\ \sigma 3-\sigma 2 = \pm\sigma y \qquad (2.7.)$$

where σy is the absolute value of the yield stress in tension or compression.

Thus the surface of yielding corresponding to the maximum shear stress theory consists of three sets of parallel planes which define a straight hexagonal prism in σ1, σ2, σ3 space whose axis coincides with the space diagonal σ1=σ2=σ3, i.e., in the positive quadrant the axes.

Cross-sections of the prism are regular hexagons (fig. 2.4.).

2.3.5. The constant elastic strain-energy-of-distortion theory

This theory is also known as the constant octahedral shearing-stress theory.

The theory is variously attributed to Huber, Henckey and Von Mises, although it is supposed to have been first mentioned by Maxwell in some private correspondence.

This theory states that plastic yielding begins when the strain energy of distortion given by W_D,
where:

$$W_D = \frac{1+\mu}{6E}\ (\sigma 1-\sigma 2)^2 + (\sigma 2-\sigma 3)^2 + (\sigma 3-\sigma 1)^2 \qquad (2.8.)$$

reaches a critical value. For a material with a pronounced yield point in simple tension, σy, we have σ1=σy and σ2=σ3=0. Subsitution into the above formula gives:

$$W_D = \frac{1+\mu}{3E}\ (\sigma y)^2$$

Thus the condition for yielding based on the distortion energy theory is:

$$(\sigma 1-\sigma 2)^2 + (\sigma 2-\sigma 3)^2 - (\sigma 3-\sigma 1)^2 = 2(\sigma y)^2 \qquad (2.9.)$$

A useful form of the theory is obtained by passing a plane through the unit points on the principal axes. Thus it is normal to a space diagonal fig. 2.4. and 2.5. $\sigma 1$, $\sigma 2$, $\sigma 3$ space i.e., principal stress space; there are thus eight such planes. The normal to each octahedral plane has the direction $\cos^{-1}(1/\sqrt{3})$ to each of the coordinate axes. Normal and shearing stresses on the octahedral plane are called "octahedral stresses".

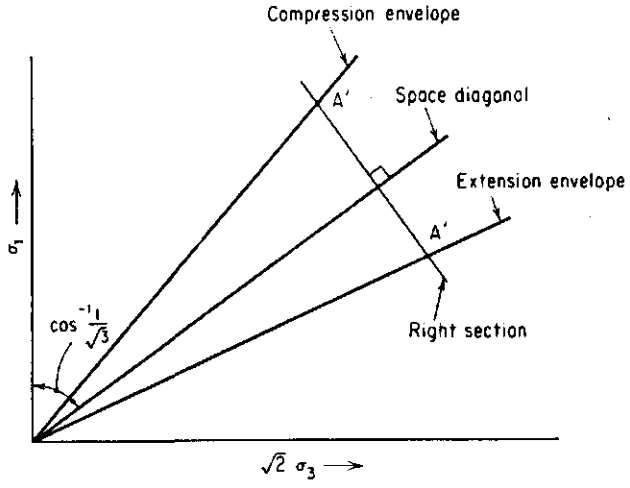

Fig. 2.5. Failure envelopes from Yong, 1975

Thus the normal octahedral stress, σoct, is:

$$\sigma oct = \frac{1}{3}(\sigma 1+\sigma 2+\sigma 3) = \frac{1}{3} J1 \qquad (2.10.)$$

where $J1 = \sigma 1+\sigma 2+\sigma 3$ = first stress invariant

The octahedral shearing stress is:

$$\sigma oct = \frac{1}{3}\left\{(\sigma 1-\sigma 2)^2 + (\sigma 2-\sigma 3)^2 + (\sigma 3-\sigma 1)^2\right\}^{\frac{1}{2}} \qquad (2.11.)$$

Thus any state of stress consisting of three principal stresses may be resolved into two component states of stress,

a) a component consisting of equal tensile (or compressive) stresses acting in all directions, and

b) a component state of stress consisting of the eight octahedral shearing stresses.

Thus from eqs. 2.9 and 2.11

$$9(\sigma oct)^2 = 2(\sigma y)^2$$

and hence:

$$\sigma oct = \frac{\sqrt{2}}{3} \sigma y \qquad (2.12)$$

Eq. 2.12 is thus a statement of the maximum energy of distortion theory. The theory further shows that at the plastic limit the octahedral shearing stress in the material is constant, which depends on the yield point of the material in simple tension or compression. The yield stresses in simple tension and compression are thus assumed to be equal.

The yielding surface defined by this theory is a straight circular cylinder whose axis coincides with the space diagonal $\sigma 1=\sigma 2=\sigma 3$.

Since planes normal to the axis of the cylinder are octahedral planes, the radius of the cylinder equals the octahedral shearing stress. The radius of the cylinder is therefore $\sqrt{2}/3\ \sigma y$. This is similar to the Von Mises yield criterion.

2.4. Failure theories

The failure theory proposed by MOHR (1900) followed the earlier work of Coulomb and Navier which considered the state of failure as a shear failure. As it turns out, both the Coulomb-Navier theory and the extended maximum shear-stress theory are special cases of the Mohr theory.

The theory which considers failure by both yielding and fracture (assuming slippage as a mode of failure) provides a functional relationship between normal and shear stresses on the failure plane, i.e.

$$\Gamma = f(\sigma)$$

where τ = shearing stress along the failure plane

σ = normal stress across the failure plane.

From the two-parameter nature of the theory the curve defined by this functional relationship may be plotted on the τ, σ-plane (fig. 2.6).

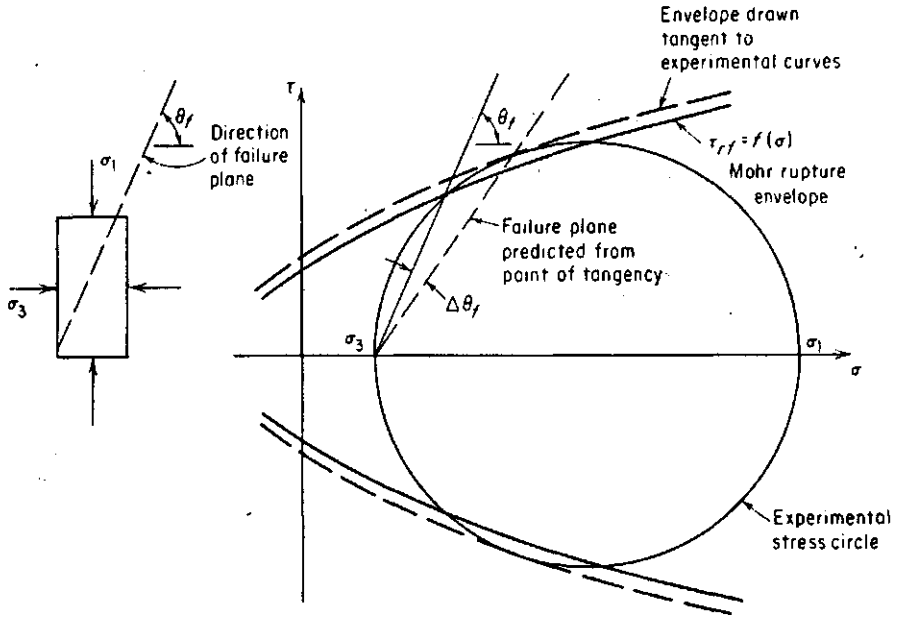

Fig. 2.6. Mohr's failure theory plotted in the Γ-σ plane from Yong, 1975

Since changing the sign of Γ merely changes the direction of failure but not the condition for it, the curve must be symmetrical about the σ-axis. The curve so obtained which is termed the Mohr rupture envelope, represents the locus of all points defining the limiting values of both components of stress (Γ and σ) in the slop planes under the different states of stress $\sigma 1$, $\sigma 2$, $\sigma 3$ to which the material may be subjected.

The Mohr envelope thus reflects a property of the material which is independent of the stresses imposed on the material.

The theory is attractive for use in studying the shear strength

of soils since there is no requirement that the material obeys Hooke's law (for ideal elastic material) or that Poisson's ratio be constant: also, the strength and stiffness of the material in tension and compression need not to be equal.

The Coulomb equation, $\Gamma = c + \sigma \tan \phi$, represents a special case of the Mohr theory of strength in which the Mohr envelope is a straight line inclined to the normal stress axis at angle cf.

The use of the Coulomb equation to represent the Mohr envelope in the Mohr diagram is called the Mohr-Coulomb theory.

Mohr's hypothesis states that failure depends upon the stresses on the slip planes and failure will take place when the obliquity of the resultant stress exceeds a certain maximum value.

It is also stated that "the elastic limit and the ultimate strength of materials are dependent on the stresses acting on the slip planes".

The Mohr representation of stresses acting on the three principal planes is shown in fig. 2.7.

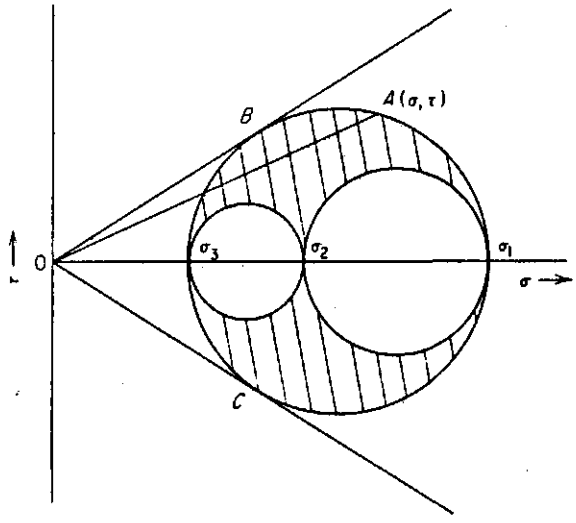

Fig. 2.7. Mohr representation of stresses in three-dimensional system from Yong, 1975

Stresses on any plane within the body must be within the shaded area. The slope of the line joining the origin and point A gives the obliquity of stress. The maximum inclination of stress will be given by the targets to the largest circle.

Failure occurs on planes where stresses are represented by points B and C. These stresses act on planes which are parallel to the diameter of the intermediate principle stress. Therefore the diameter of the largest Mohr circle and the magnitude of the stresses at points B and C are independent of the intermediate principal stress, $\sigma 2$. With the assumption that $\sigma 2$ is the intermediate principal stress, the largest of three circles representing the limiting state of stress will be of diameters $(\sigma 1-\sigma 3)$ and centred at $(\sigma 1+\sigma 3)/2$ along the σ-axis, as seen in fig. 2.6, taking due account of the algebraic sign of the stresses. Since the two parallel sets of slip planes which occur when an isotropic specimen has been stressed slightly beyond the plastic limit by a state of homogeneous stress are symmetrically inclined with respect to the directions in which the major and minor principal stresses act, and the two plane systems intersect each other along the direction in which the intermediate principal stress acts, Mohr assumed that the intermediate principal stress is without influence on the failure of a material.

Accordingly, some point on the perimeter of the circle of diameter $(\sigma 1-\sigma 3)$ must represent the limiting stress condition.

The theory thus affords a method of devising a failure theory for a specific material, i.e., establishing its Mohr rupture envelope, from actual test results.

In practice a series of similar specimens is subjected to different stresses and brought to failure (as in the triaxial test).

The various Mohr's stress circles are plotted for the limiting states of stress and the unique failure stress on the failure plane for each test is taken as the point of common tangency between a smooth limiting curve (or envelope) and the various $(\sigma 1-\sigma 3)$ circles.

By taking the points of common tangency as representative of the σ and Γ stresses on the failure plane, a state of homogeneous stress in an isotropic material is assumed. Due to experimental

shortcomings, however, one may not necessarily obtain a state of homogeneous stress and thus the inferred stresses at the point of common tangency for the envelope, obtained experimentally, will not in all likelihood represent the actual stresses on the failure plane. It follows then that the predicted location of the failure plane, based on the common tangency points might be in error.

The possible discrepancy between the actual Mohr rupture envelope and an experimentally obtained envelope is shown on fig. 2.6.

Actual Mohr rupture envelopes are often curves. However, for soils the curvature is usually not great and it has proved useful to approximate the envelope by a straight line, at least over a limited range of normal stress.

The equation of a straight line in the Γ, σ-plane is the Coulomb equation $\Gamma=S=C+\sigma \tan \phi$.

From fig. 2.8. the following formula may be derived:

$$R = \frac{\sigma 1-\sigma 3}{2} = c \cos \phi + (\frac{\sigma 1+\sigma 3}{2}) \sin \phi \qquad (2.13)$$

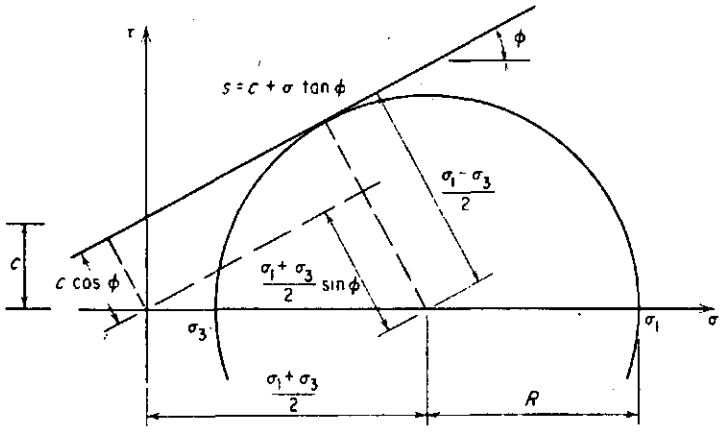

Fig. 2.8. Properties of a straight-line Mohr envelope, σ1 and σ3 are limiting effective stresses at failure. Compressive stresses considered positive in deriving eq. 8.13. from Yong, 1975

The parameters c and ϕ in eq. 2.13 are the analytical parameters of "cohesion" and "friction angle". They are a direct consequence of the application of the Mohr-Coulomb theory and need not bear any physical semblance to the real material properties of cohesion and friction of soil.

When the physical conditions of failure in the test specimen are met, e.g. little or no volume change, development of failure plane, etc., the analytical parameters will more closely correspond and reflect the physical material (mechanistic) parameters.

Eq. 2.13 may be manipulated in many ways to state the failure criterion in various forms. For example, by adding $\sigma 3 \sin\phi$ to both sides of the equation and by rearranging terms, we will obtain:

$$\frac{1}{2}(\sigma 1-\sigma 3)(1-\sin\phi) = c\cos\phi + \sigma 3 \sin\phi \qquad (2.14)$$

Eq. 2.14 which was used by Skempton and Bishop gives straight lines when $(\sigma 1-\sigma 3)/2$ is plotted against 3. By multiplying both sides of eq. 2.13 by 2 and rearranging terms, we get:

$$\sigma 1(1-\sin\phi) = 2c\cos\phi + \sigma 3 (1+\sin\phi) \qquad (2.15)$$

which gives straight lines when $\sigma 1$ is plotted against $\sigma 3$. This last equation has been used as a plotting method by Rendulic and more recently by HENKEL (1959).

Expressed in its most general form, the failure surface corresponding to the Mohr-Coulomb condition to failure is:

$$\left[(\sigma 1-\sigma 2)^2 - \{2c\cos\phi + (\sigma 1+\sigma 2)\sin\phi\}^2\right] X$$
$$\left[(\sigma 2-\sigma 3)^2 - \{2c\cos\phi + (\sigma 2+\sigma 3)\sin\phi\}^2\right] X$$
$$\left[(\sigma 3-\sigma 1)^2 - \{2c\cos\phi + (\sigma 3+\sigma 1)\sin\phi\}^2\right] = 0 \qquad (2.16)$$

The failure surface defined by eq. 2.16 is a pyramid with the space diagonal $\sigma 1=\sigma 2=\sigma 3$ as axis and a cross-section which is an irregular hexagon with nonparallel sides of equal length (see fig. 2.9).

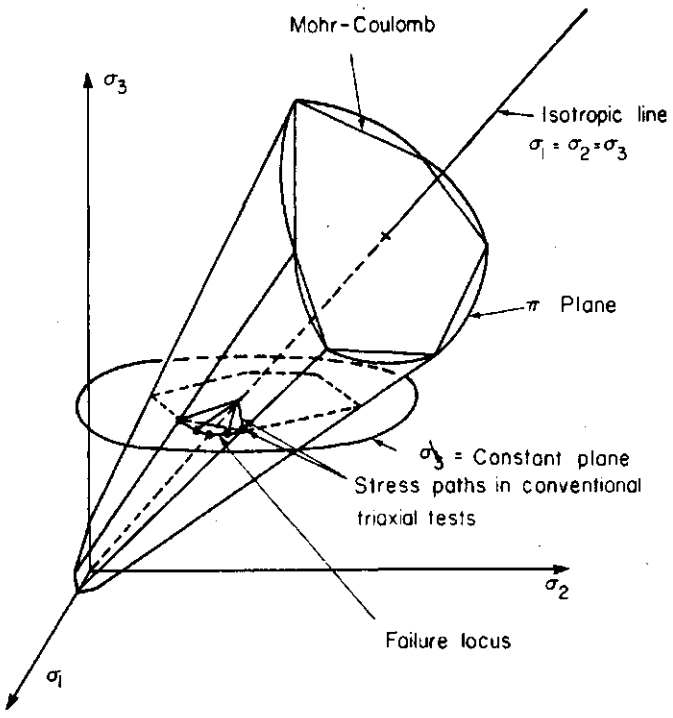

Fig. 2.9. Mohr-Coulomb failure surface in principal stress space showing stress paths in conventional triaxial tests. (from YONG, 1975)

The projection of this irregular hexagon on the plane $\sigma 1+\sigma 2+\sigma 3$ = constant (i.e. a plane at night angles to the space diagonal or an octahedral plane) is shown in fig. 2.10. The three criteria are seen to coincide for compressive tests but the strength in a tensile test is seen to be less for the Mohr-Coulomb failure theory.

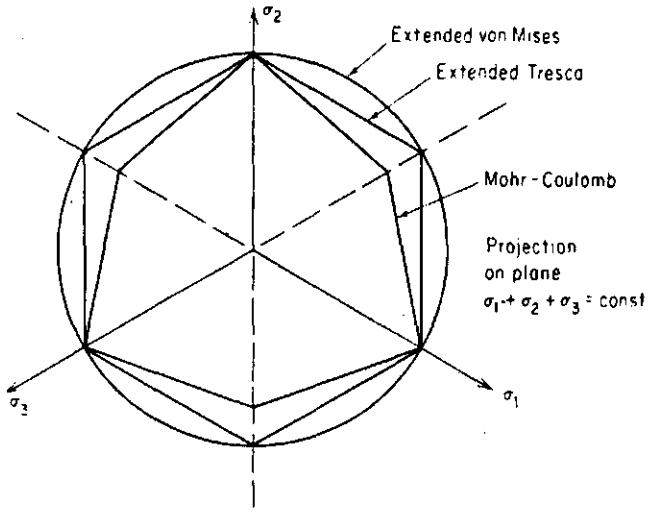

Fig. 2.10. Failure surfaces-Mohr Coulomb and extended yield criteria. (from YONG, 1975)

More details about soil behaviour and failure laws can be found in the work of SCHOFIELD (1968) and KURTAY (1970).

LITERATURE CHAPTER 2.

KURTAY, T. and A.R. REECE, 1970. Plasticity theory and critical state soil mechanics. Journal of Terramechanics, Vol. 7, nos. 3 and 4. pp 23 to 56. Pergamon Press., Printed in Great Britain.

LAMBE T. WILLIAM and ROBERT V. WHITMAN, 1969. Soil Mechanics - Massachusetts Institute of Technology. John Wiley and Sons Inc. New York.

SCHOFIELD, ANDREW and PETER WROTH, 1968. Critical State Soil Mechanics. Mc. Graw-Hill. London

YONG, R.N. and B.P. WANKENTIN, 1975. Soil Properties and Behaviour. Developments in Geotechnical engineering. Vol. 5 - Elsevier Scientific Publishing Company.

3. METHODS FOR MEASURING SHEAR STRENGTH OF SOILS

3.1. P e n e t r o m e t e r

3.1.1. Principle

The first penetrometer developed was a cone test which utilized a cone with an apex angle of 90^{o}, resting on a cohesive soil sample and progressively loaded (fig. 3.1.).

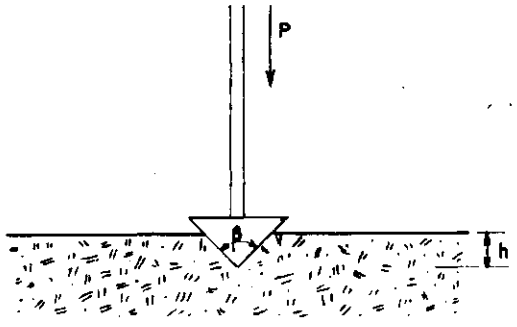

Fig. 3.1. Principle of operation of the pocket penetrometer. (from SANGLERAT, 1972)

The depth of penetration into the sample for each load increment was measured. The area A of the imprint of the cone into the sample was calculated from the measured depth of penetration. The ratio of the load to the surface area of the imprint was a constant, called the soil resistance to the cone penetration and measured in kg/cm^2 or in bar.

The ratio increased as the strength of the clay increased, so that:

$kc=P/A$ where k=constant, c=cohesion, P=load and A=area line imprint

This may also be written as:

$$P = \Pi \, kc \, (h \tan \beta/2)^2$$

where β = apex angle of the cone, and for $\beta = 90^{o}$ $P = \Pi \, kc \, h^2$

From experimental data, it is possible to determine the value of the constant k, and once it is known, cohesion c may be obtained.

3.1.2. The static penetrometer

Here the cone is driven into the soil with a constant speed and the resistance to penetration is measured.

3.1.2.1. Influence of penetration speed on penetration resistance. On clay the influence of the penetration speed has a considerable influence on the penetration resistance. FREITAG (1968) found a relationship between strength ratio and penetration speed as shown in fig. 3.2., where the strength ratio is the soil strength measured at a speed of 180 cm/min devided by the strength at actual speed.

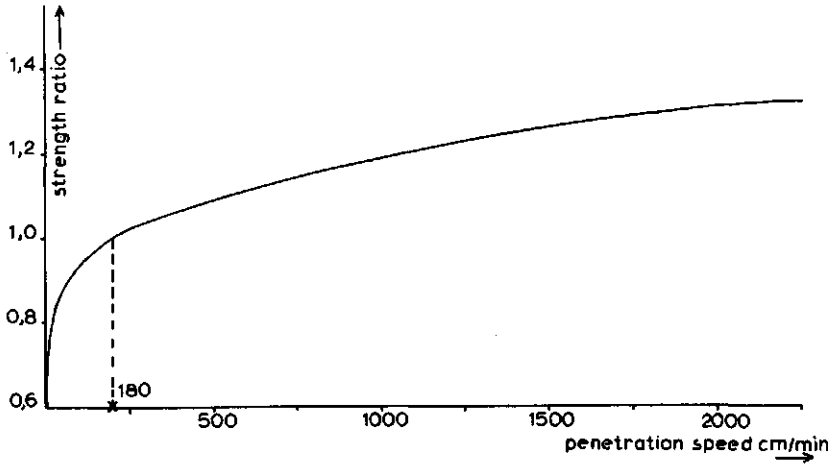

Fig. 3.2. Strength ratio versus penetration speed from FREITAG (1968)

Normally the penetration speed is less than ± 50 cm/min in research measurements and the influence of different penetration speed is negliable.

However one should prefer a mechanical operated penetrometer which is driven into the soil at a constant speed and where the resistance is registrated automatically.

3.1.2.2. Effect of tip angle and surface material on the cone index. GILL (1968) found an influence of the tip angle of the cone on the cone index (penetration-resistance force devided by the maximum cross sectional area of the penetrometer tip) fig. 3.3.

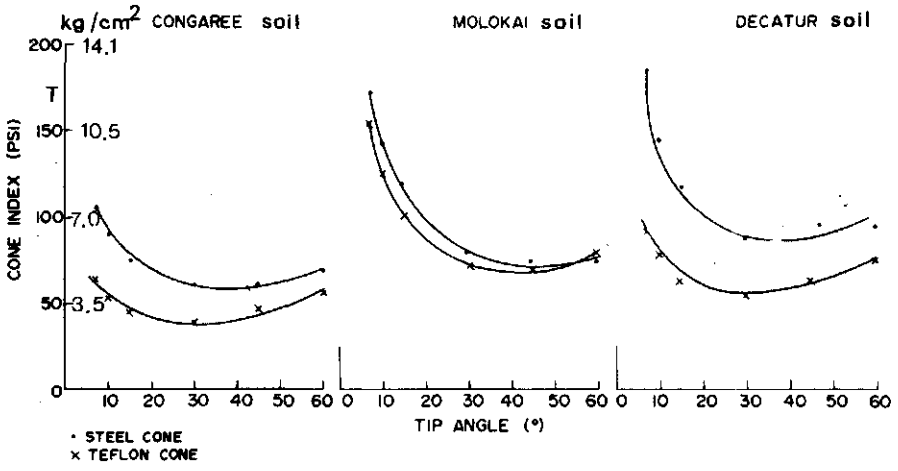

Fig. 3.3. Effect of tip angle and surface material on cone index from GILL, 1968

The U.S. Army Waterways Experiment Station at Vicksburg, Miss. reported data to show that tip shape had little influence on the cone index values of soils. In U.S. the constante-rate type of soil penetrometer with tip angle of 30^{o} and maximum surface area of 0.5 sq. in- is often used. In Europe a cone with a tip angle of 60^{o} and a maximum surface area of 10 cm^2 is more common.

One must always be aware of the difference between friction on the shaft and the resistance to the cone itself when the values of two different types of penetrometers are compared.

3.1.2.3. Correlation between cone resistance, the cohesion and angle of internal friction. In agricultural soil mechanical problems we are mostly interested in the first 2 or 3 meters of the soil. There-

fore the de Beer theory for the interpretation of penetrometer test data for shallow foundations may be of interest.

The de Beer theory is based on the formulas derived by K. Buisman of the Delft Laboratory of soil mechanics which, in turn, were derived from the Prandtl-Caquot equations (SANGLERAT, 1972).

For practical purposes the resistance at the point of the penetrometer could be expressed by the following equation (from experimental data of Keverling Buisman, Delft)

$$qc = 1.3 \left[po \tan^2 \left(\frac{\Pi}{4}+\frac{\phi}{2}\right) e^{\Pi \tan\phi} + \frac{c}{\tan\phi} \left\{ \tan^2 \left(\frac{\Pi}{4}+\frac{\phi}{2}\right) e^{\Pi \tan\phi} - 1 \right\} \right] \qquad \text{eg. 1}$$

where qc = cone resistance

po = overburden pressure at the same level of the cone.

The empirical coefficient of 1.3 is due to the conical shape of the penetrometer point (10.0 - cm^2 section, apex angle of 60^o). When dealing with sands, c=o and knowing the value of qc, the angle of internal friction may be calculated from equation 1 .

When dealing with homogeneous cohesive material, the value of qc must be determined at two locations at different depths. This gives a set of two equations with two unknowns, namely, the cohesion c and the angle of shearing resistance ϕ. These two unknowns can theoretically be calculated. De Beer has produced practical calculation methods for the solution of the equations.

Other practical values for the cohesion of normally consolidated sandy clay are between qc/10 and qc/20, depending on the type of penetrometer used.

From Sanglerat page 201,
"It has been shown here how important it is to know the type of penetrometer used in field tests to determine by which formula the cohesion may be evaluated".

For deeper penetration tests de failure surface above and below the cone is very similar tot that presented in fig. 3.4.

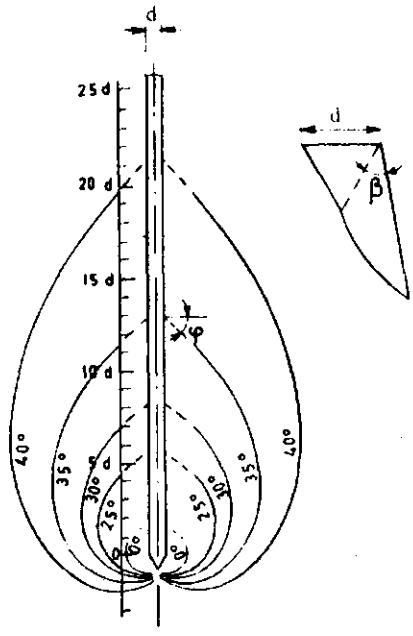

Fig. 3.4. Critical embedment: logarithmic spiral equation $\gamma = d$ $\gamma = d\, e^{\beta \tan \phi}$ from SANGLERAT (1972)

The print resistance is actually equal to twice the value obtained from the Buisman-Prandtl formula (eq. [1]). It can therefore be concluded that the failures occuring both above and below the point each contribute about 50% of the resistance of penetration of the cone.

For cohesive soils $\phi = 0$ one has found the formula

$$cu = (qc - Pb) / 13{,}4$$

where qc = priot resistance of the penetrometer in bar

cu = cohesion

Pb = overburden pressure at the depth of the test.

At shallow depths, the value of Pb is often so small that it may be ignored.

The coefficient of 13.4 used with the data of the penetrometer tests gives results which are in very good agreement with those of the vane shear tests.

3.1.3. The dynamic penetrometer - Standard Penetration test

3.1.3.1. P r i n c i p l e. The most widely used penetration test is the "standard penetration test", which consists of driving a spoon into the ground by dropping a 63,4 kg weight from a height of 0,76 m (LAMBE and WHITMAN, 1969).

The penetration resistance is reported in number of blows of the weight to drive the spoon 0,3 m.

Tabel 3.1. presents a correlation of standard penetration resistance with relative density of sand and a correlation of penetration resistance with unconfined compressive strength of clay.

Tabel 3.1. Standard Penetration Test

Relative Density of Sand			Strength of Clay		
Penetration Resistance N (blowd/ft)	Relative Density	%	Penetration Resistance N (blows/ft)	Unconfined Compressive Strength (tons/ft^2)	Consistency
0-4	Very loose	0-15	< 2	< 0.25	Very soft
4-10	Loose	15-35	2-4	0.25-0.50	Soft
10-30	Medium	35-65	4-8	0.50-1.00	Medium
30-50	Dense	65-85	8-15	1.00-2.00	Stiff
>50	Very dense	85-100	15-30	2.00-4.00	Very stiff
			>30	>4.00	Hard

From Terzaghi and Peck, 1948. From Lambe, 1969

$$\text{Relative density } D = \frac{e_{max} - e}{e_{max} - e_{min}} \times 100\%$$

$$e = \text{void ratio} = \frac{\text{void volume}}{\text{solid volume}}$$

e_{min} = void ratio of soil in densest condition

e_{max} = void ratio of soil in loosest condition

e = actual void ratio

The standard penetration test is a very valuable method of soil investigation. It should, however, be used only as a quide, because there are many reasons why the results are only approximate.

As laboratory tests show the penetration resistance depends on factors other than relative density. The penetration resistance depends on the confining stress and or the type of sand. The influence of sand type on penetration resistance is particularly large at low densities.

Another factor that may have a marked influence on the penetration resistance in a sand is the pore pressure condition during the measuring operation.

Experience has shown that the determination of shear strength of a clay from the penetration test can be very unreliable (LAMBE and WHITMAN, 1969).

Fig. 3.5. shows the correlation between friction angle and penetration resistance for a sand (Lambe and Whitman).

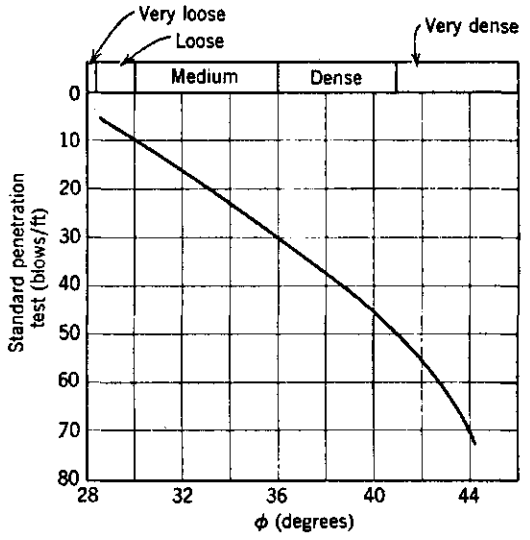

Fig. 3.5. Correlation between friction angle and penetration resistance (From PECK, HANSEN and THORNBURN, 1953). From LAMBE, 1969

3.1.3.2. Correlation between N-values of the standard penetration test and dynamic shear moduli. Dynamic shear modulus is one of the most important parameters in the response analyses of soil deposits during an earthquake.

Because the standard penetration test is a simple and rapid means of soil exploration, extensive efforts have been made to correlate the results of the test with a number of important soil properties which otherwise require laborious sampling and testing techniques for their determinations.

OHSAKI and IRVASAKI (1973) report that from statistical analyses of accumulated data on dynamic characteristics of various soil deposits measured by means of seismic exploration it has been found that shear moduli for small shear strain level are well correlated with N-values of the standard penetration test, and that their interrelation may be expressed by a simple, approximate eg.

$$G = 1200\ N^{0.8}\ \text{(tons/sq. meter)}$$

where:

G = shear modulus

N = n-values of the standard penetration test (blows/ft)

OHTA ET ALL (1972) found $G = 1390\ N^{0.72}$

They found for different soils different correlation coefficients and other values for the coefficients (see fig. 3.6).

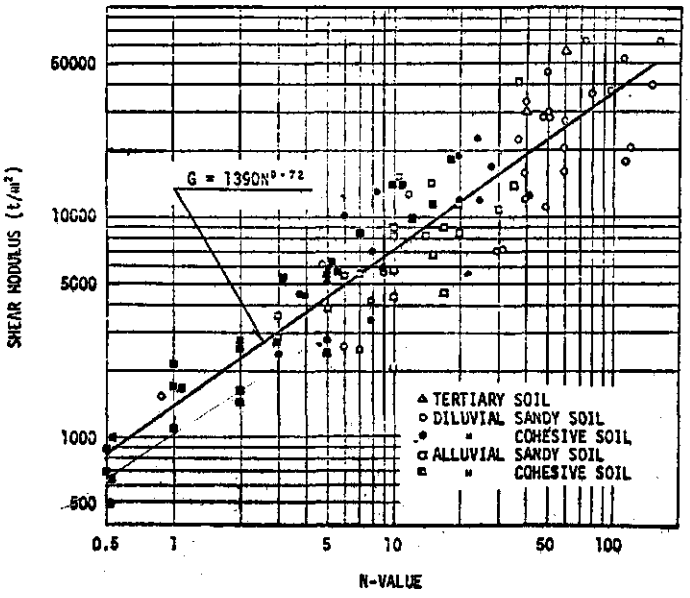

Fig. 3.6. Shear moduli and N-values (OHTA ET AL, 1972) from OHSAKI, 1973

Relationships between Poisson's ratio and shear modulus under dynamic and static conditions have also been pointed out by Ohsaki and Iwasaki.

3.1.4. Summary

In present publications the principal approach encountered is to relate the penetrometer resistance for a certain type of soil on a specific location with the cohesion and angle of internal friction or other soil mechanical parameters which are determined with other measuring devices (i.e. uniaxial tests, unconfined compression test, vane tests, shear tests).

This for the sake of rapideness and cheapness of the penetrometer test compared with the other tests.

For static soil mechanical parameters the static penetrometer is preferable above the dynamic penetrometer because of the lack of theoretical background for the dynamic penetrometer.

For dynamic soil mechanical parameters one can use the dynamic penetrometer as showed OHSAKI (1973).

LITERATURE PENETROMETER CHAPTER 3.1.

FREITAG, H.R., 1968. Penetration tests for Soil Measurements Transactions of the ASAE, vol. 11 no. 6, pp. 750-753.

GILL, WILLIAM R., 1968. Influence of compaction hardening of Soil on Penetration Resistance. Transactions of the ASAE vol 11. no. 6, pp. 741-745.

LAMBE, T. WILLIAM and ROBERT V. WHITMAN, 1969. Soil Mechanics - John Wiley and Sons, Inc. London.

OHSAKI, YONIHIKO and RYOJI IWASAKI, 1973. On dynamic shear moduli and Poisson's ratio's of soil deposits - Soils and Foundations. Vol. 13 no. 4, dec. 1973.

SANGLERAT, G, 1972. The penetrometer and soil exploration. Elsevier Scientific Publishing Company, Amsterdam.

3.2. V a n e - t e s t

3.2.1. Principle

The vane is forced into the ground and then the torque required to rotate the vane is measured. The shear strength is determined from the torque required to shear the soil along the vertical and horizontal edges of the vane (see fig. 3.7).

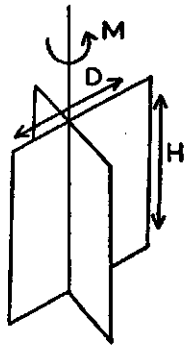

$M = \Gamma(\frac{1}{2}\pi D^2 H + \frac{1}{6}\pi D^3)$ where

M = torque to shear in soil kg/cm

Γ = shearing stress kg/cm^2

D = diameter vane cm

H = height of vane blades cm

Fig. 3.7. Vane blades

The two chief advantages of the vane test are

1) the test is conducted in situ and avoids the problems of stress release and sample disturbance
2) the test is relatively inexpensive compared with conventional tube sampling and laboratory testing.

The restrictions of the test are

1) it can only be used in rather uniform cohesive soils which are fully saturated
2) it does not yield samples by which an accurate identification of the materials in a boring profile can be made

3) it imposes a failure surface on the soil which may not be relevant to the problem being studied (EDEN, 1966)
4) inserting the vane into the soil disturbs the soil or the "undisturbed sample".

With the vane test one cannot apply a normal load to the soil. So the shear strength is only measured with normal zero, hence one cannot distinguish between cohesion and friction components in the shear strength formula.

Therefore the vane test is only used in cohesive soils with ϕ supposed to be zero and so the shear strength is completely due to the cohesion.

Fig. 3.8. gives different types of vanes.

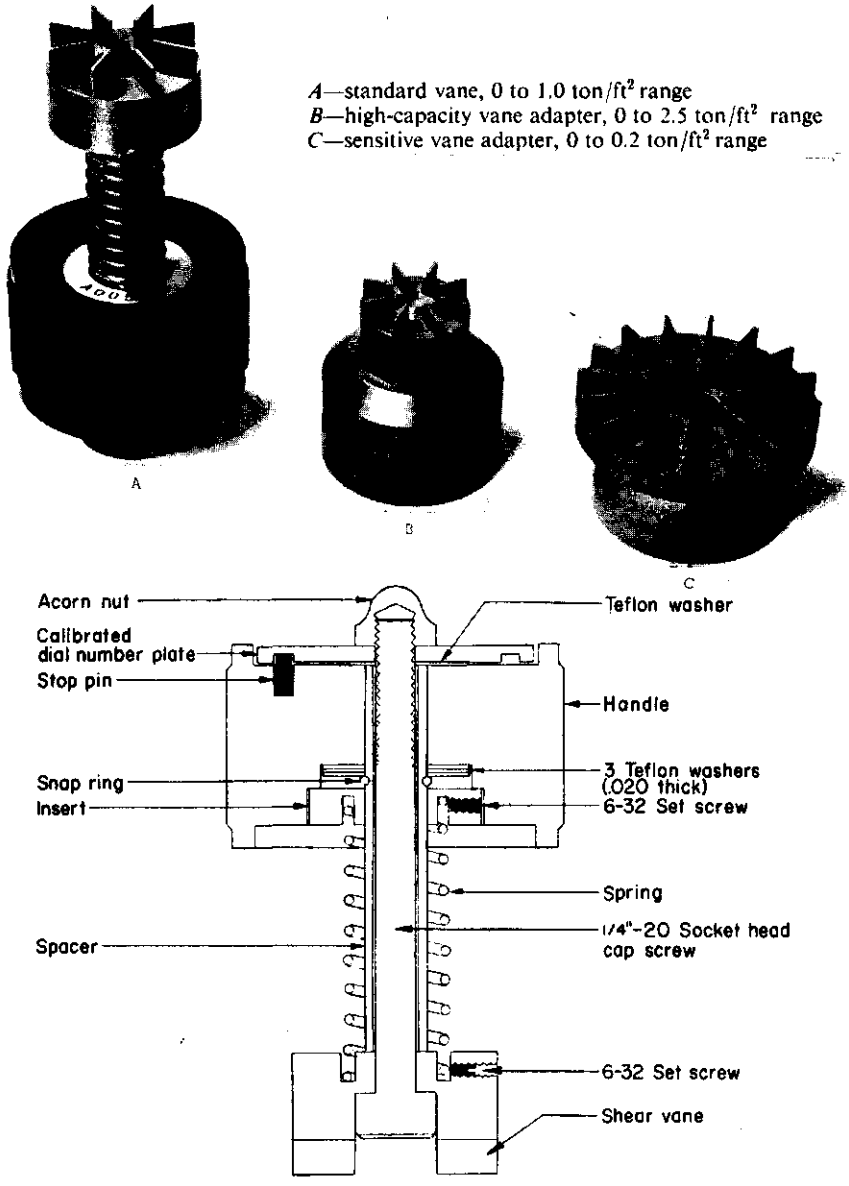

Fig. 3.8. Hand-operated torsional vane shear device from SIBLEY (1966)

3.2.2. Influence of rate of loading on the vane shear strength

SIBLEY (1966) found the relationship between shear strength and rate of stress as showed in fig. 3.9.

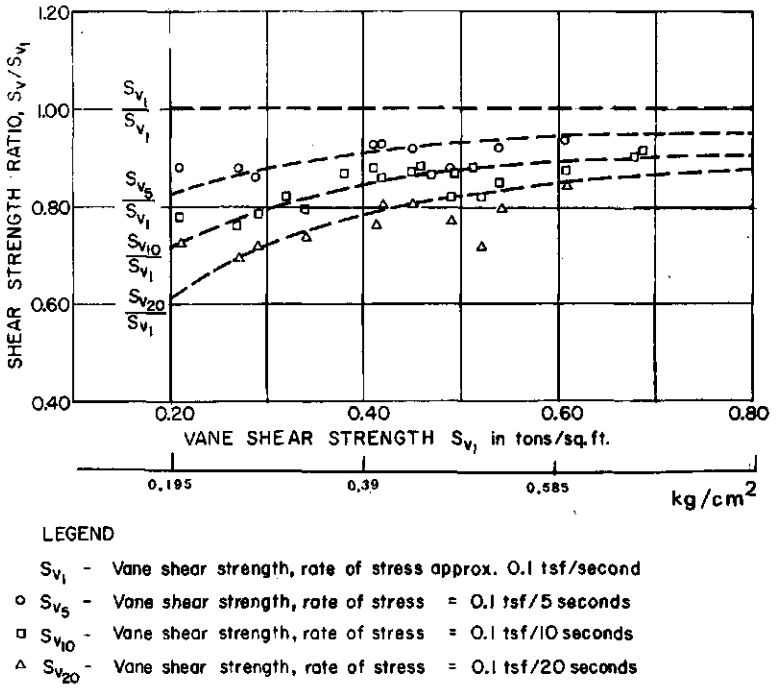

Fig. 3.9. Relationship between torsional vane shear strength and rate of stress, Bootlegger Cove clay (from SIBLEY, 1966)

A high loading rate gives a higher strength especially in soils with a low shear strength.

LITERATURE VANE TEST CHAPTER 3.2.

EDEN, W.J. An evaluation of the field vane test in sensitive clay. Vane shear and Cone Penetration Resistance Testing of In-Situ Soils, ASTM STP 399, Am. Soc. Testing Mats. 1966, p.8.

SIBLEY, E.A. and G. YAMANE. A simple shear test for saturated cohesive soils. Vane shear and cone penetration resistance testing of in-situ soils, ASTM. STP 399, Am. Soc. Testing Mats. 1966, p.39.

3.3. S h e a r a n n u l u s

This instrument has been developed in order to overcome the fact that the outermost elements must move considerable further than those in the center of the vane. Shearing stress is easily calculated for a narrow annulus by using polar coordinates (agricultural handbook no. 316 U.S.D.A.).

An elemental area is given by

$$r\, d\theta\, dr$$

and assuming a constant shear stress τ acting on the annulus area, the force on the elemental area is

$$\tau\, r\, d\theta\, dr$$

The force acts at a distance r from the center so that the moment at the center of the annulus is

$$S r^2\, d\theta\, dr$$

Integrating over the appropriate area gives the total moment, which has the form

$$M = \int_{r2}^{r1} \int_{0}^{2\Pi} S r^2\, d\theta\, dr$$

Performing the integration gives

$$M = \frac{2\Pi S\ (r1^3 - r2^3)}{3}$$

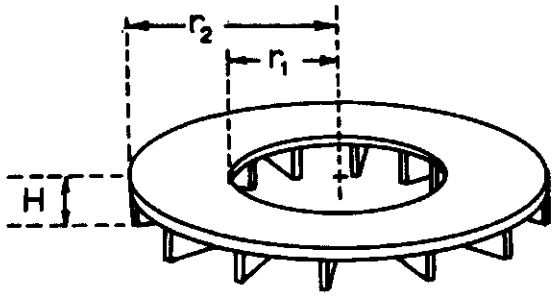

Fig. 3.10. Shear annulus

In fact one should also count for the sidewall friction

$\{2(2\pi r_1 x r_1 x H) + 2(2\pi r_2 x r_2 x H)\}P$, where

H = depth of annulus in the soil

P = metal to soil friction factor or when the ring is open to one side the shear strength of the soil.

KUIPERS (1966) found that an oiled annulus gave a value for the cohesion that was $\pm$ 10% lower than that of a not oiled one.

COHRON (1962) discussed the problem of the uniform normal stress distribution under a loaded shear head. He concluded that the assumption of uniform pressure distribution might lead to errors of the order of $\pm$ 25%. The shear vane data, however, reveal no such startling discrepancies in the test sand, when compared with the results of the translational shear test. Therefore, for all practical purposes, the assumption of uniform pressure is a valid one.

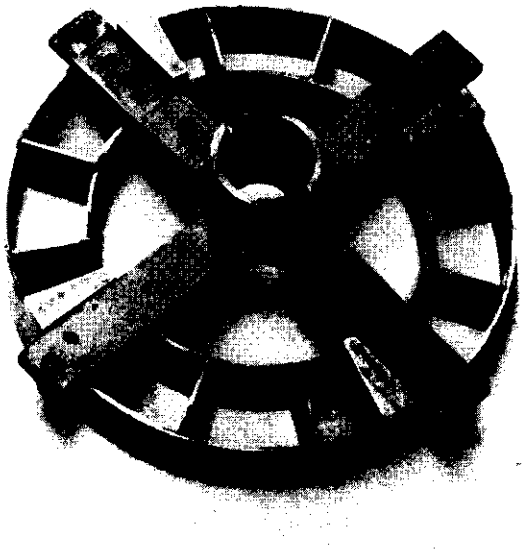

Fig. 3.11. Normal annulus with cross and coupling. From KUIPERS (1966)

3.4. Solid shearhead

The shearhead is a disc with grousers. On the disc one can apply a normal load. With this instrument one can find the shear strength under different normal load conditions and so the cohesion and the angle of internal friction can be found (COHEN, 1962).

The formula for the shear strength

$$\Gamma = \frac{3M}{2\pi R^3}$$

where

Γ = shear strength

M = torque to shear in the soil

R = diameter of disc (see fig. 3.12)

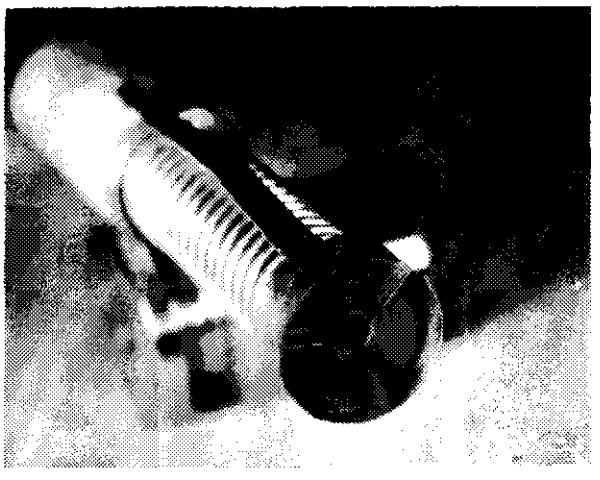

Fig. 3.12. Torsional shearhead. From BAILEY (1965)

LITERATURE SHEAR ANNULUS AND SOLID SHEARHEAD. Chapter 3.3. and 3.4.

AGRICULTURAL HANDBOOK no. 316 - Soil dynamics in tillage and traction. United States department of agriculure.

BAILEY, A.C. and J.A. WEBER. Comparison of Methods of Measuring Soil Shear Strength Using Artificial Soils - Transactions of the ASAE - vol. 8 no. 2, p. 153.

COHNON, GERALD T. The soil sheargraph. Presentation at the 1962 annual Meeting American society of agricultural Engineering.

KUIPERS, H and B. KROESBERGEN. The significance of moisture content, pore space, method of sample preparation and type of shear annulus used on laboratory torsional shear testing of soils. Journal of Terramechanics, 1966, vol. 3, no. 4, pp. 17 to 28.

3.5. Direct shear test

The direct shear test is the oldest form of shear test upon soil, first used by COULOMB in 1776. The essential elements of the direct shear apparatus are shown by the schematic diagram in fig. 3.13. The soil is held in a box that is split across its middle. A confining force is applied and then a shear force is applied so as to cause relative displacement between the two parts of the box. The magnitude of the shear forces is recorded as a function of the shear displacement, and usually the change in thickness of the soil specimen is also recorded.

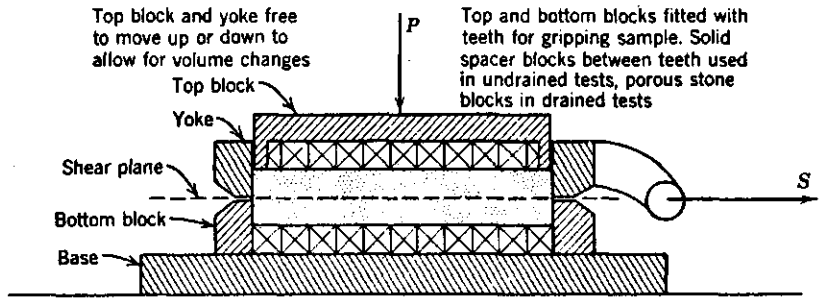

Fig. 3.13. Cross section through direct shear box (B.K. Hough - Basic Soils Engineering. Copyright, 1957 the Ronald Press Co. N.Y.). From LAMBE, 1969

The shear box may be either square of circular in plan view. Typically the box will be 20-25 cm^2 and about 2,5 cm in height. The normal load P is applied either by a loading press or by means of dead weights. In most devices the normal stress will range from 0 to about 10 kg/cm^2. The shear force S is applied either by dead weights (stress controlled test) or by a motor acting through gears (strain controlled test).

When testing dry soils the duration of the direct shear test is similar to that of the triaxial test.

The shear box can also be used in the field (see fig. 3.15).

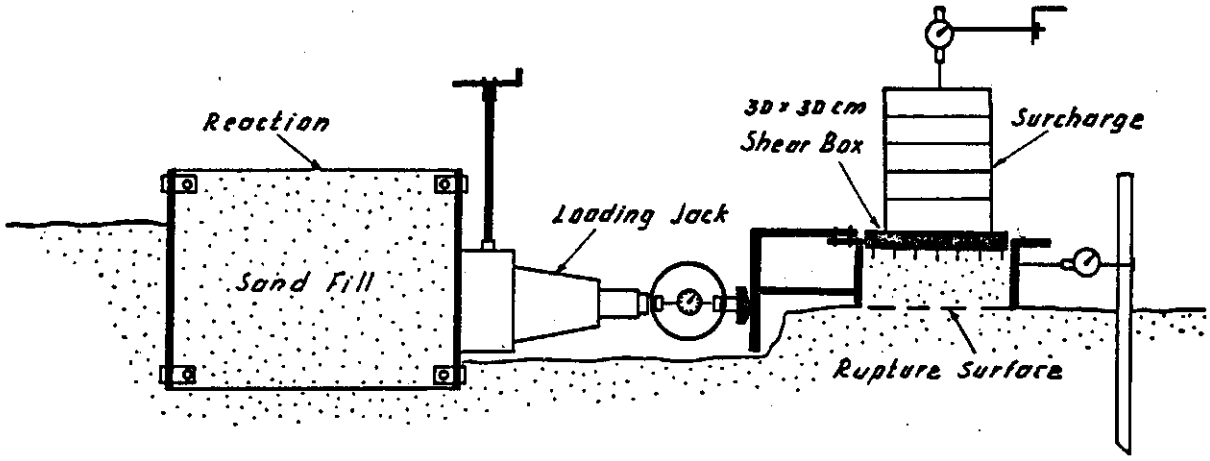

Fig. 3.15. Scheme used for field direct shear tests from ZEITLER, 1966

LITERATURE DIRECT SHEAR BOX. Chapter 3.5.

LAMBE and WHITMAN, 1969. Soil Mechanics. Massachusetts Institute of of Technology John Wiley and Sons, Inc. New York.

ZEITLER, JOSEPH G. and Y. NEGNI, 1966. Study of horizontal and vertical loading tests on a sand. Technion - Israel institute of technology. Faculty of civil engineering. Publication no. 31.

3.6. T r i a x i a l t e s t

3.6.1. Types of triaxial test

BISHOP and HENKEL (1957)

i) undrained tests. No drainage, and hence no dissipation of pore pressure, is permitted during the application of the all-round stress. No drainage is allowed during the application of the deviator stress.

ii) consolidated-undrained tests. Drainage is permitted during the application of the all-round stress, so that the sample is fully consolidated under this pressure. No drainage is allowed during the application of the deviator stress.

iii) drained tests. Drainage is permitted throughout the test, so that full consolidation occurs under the all-round stress and no excess pore pressure is set up during the application of the deviator stress.

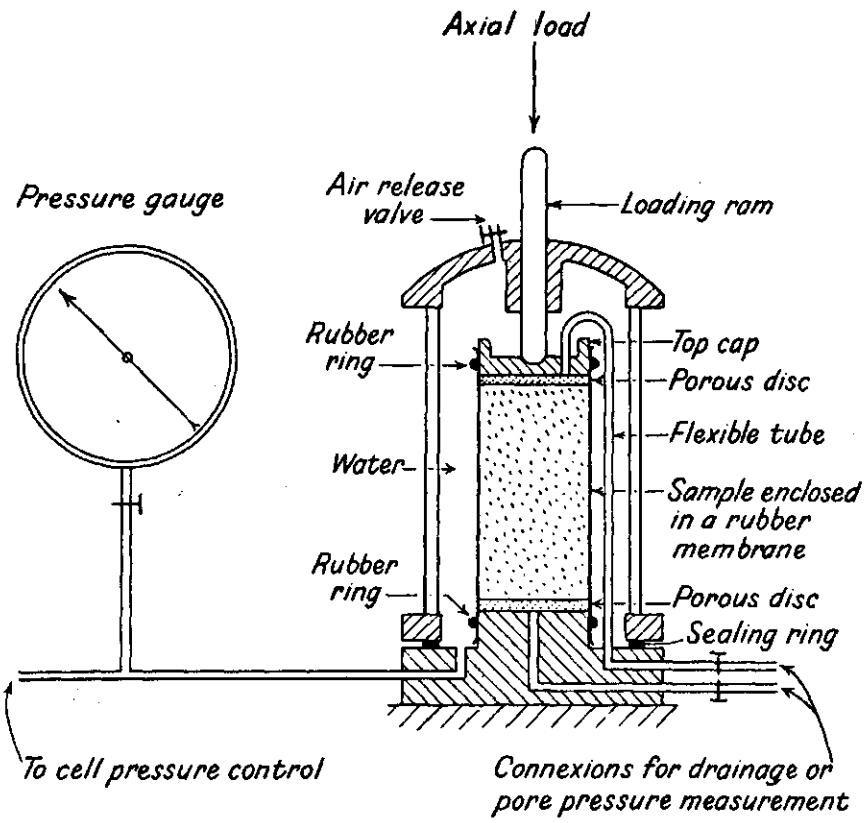

Fig. 3.16. Diagrammatic layout of the triaxial test

3.6.2. Undrained test on saturated cohesive soils

The test is carried out on undisturbed samples of clay, silt and peat as a measure of the strength of the natural ground; and on remoulded samples of clay when measuring sensitivity or carrying out model tests in the laboratory.

The deviator stress as failure is found to be indepent of the cell pressure (with the exception of fissured clays and compact silts at low cell pressure).

If shear strength is expressed as a function of total normal stress by Coulomb's empirical law:

$$\Gamma f = cu + \sigma tg\phi 4$$

cu = apparent cohesion
$\phi 4$ = angle of shearing resistance

with respect to changes in total stress

Then it follows that, in this particular case

$$\phi 4 = 0$$

$$cu = \tfrac{1}{2} (\sigma 1 - \sigma 3)$$

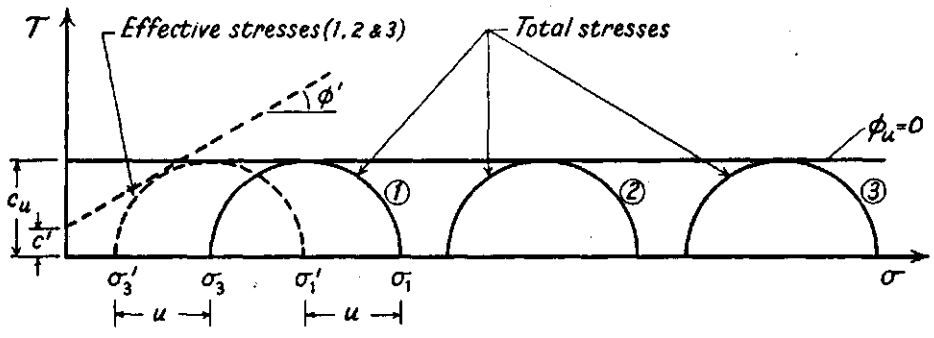

Fig. 3.17. Mohr stress circles for undrained tests on saturated cohesive soils

The shear strength of the soil, expressed as the apparent cohesion, is used in a stability analysis carried out in terms of total stress, which, for this type of soil, is known as the $\phi = 0$ analysis.

For saturated clays both the major principal effective stress $\sigma_1^1 = (\sigma 1-u)$ and the minor principal effective stress σ_3^1 $(=\sigma 3-u)$ are independent of the magnitude of the cell pressure applied (u = pore pressure). Hence only one effective stress circle is obtained from these tests and the shape of the failure envelope in terms of effective stress cannot be determined.

Because the sample as used here has another stress history than the soil in situ no pore-pressure measurements are made during undrained tests on saturated samples.

The failure stress is taken to be the maximum deviation stress which te sample can withstand.

Where the stress-strain curve has a pronounced peak this value is unambiguous. In some soils which have softened after being heavily consolidated, and in remoulded soils, failure takes the form of plastic yield at a constant stress and occurs only after very large axial strains. Termination of the test at an arbitrary strain of 10% or even 20% may lead to an underestimate of strength.

3.6.3. Undrained test on partly saturated cohesive soils

The deviator stress at failure is found to increase with cell presse. This increase becomes progressively smaller as the air in the voids is compressed and passes into solution and ceases when the stresses are large enough to cause full saturation. The failure envelope expressed in terms of total stress is thus non-linear, and values of Cu and $\phi 4$ can be quoted only for specific ranges of pressure (see fig. 3.18).

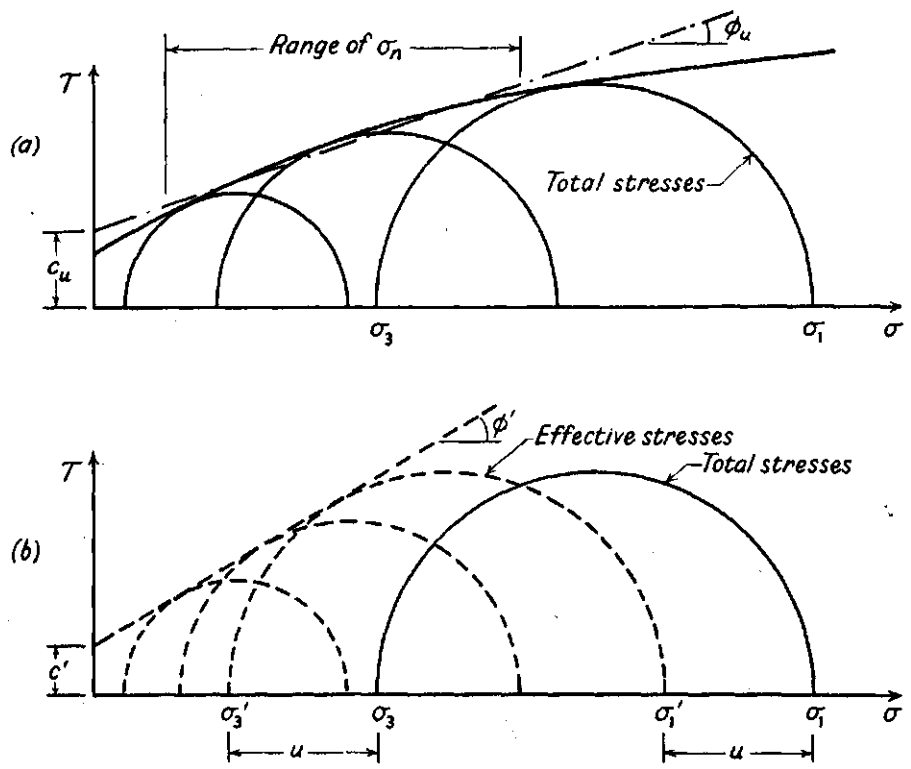

Fig. 3.18. Mohr stress circles for undrained tests on partly saturated soil. (a) total stresses, (b) effective stresses

If the pore pressure is measured during the test, as is now more usual, the failure envelope can be expressed in terms of effective stress (fig. (b)), and is found to approximate very closely to a straight line over a wide range of stress.

Apparent departures from linearity are usually found to be due to small differences in water content between the three or four samples used to define the envelope.

3.6.4. Consolidated-undrained test on saturated soils

In the standard test the sample is allowed to consolidate under a cell pressure of known magnitude (P), the three principal stresses thus being equal.

Then the sample is sheared under undrained conditions by applying

an axial load. As in the case of the undrained test, the cell pressure at which the sample is sheared does not influence the strength (except of dilatant sands).

The test result, in terms of total stresses, may thus be expressed as the value of cu, the apparent cohesion, plotted against consolidation pressure P. For normally consolidated samples the ratio cu/P is found to be a constant, its value depending on the soil type. However, undrained triaxial tests and vane tests on strata existing in nature in a normally consolidated state lead to a lower estimate of the ratio cu/P than is found in samples consolidated under equal all-round pressure in laboratory. The difference increases as the plasticity index decreases and may be attributed mainly to two causes.

1) A naturally deposited sediment is consolidated under conditions of no lateral displacement and hence with a lateral effective stress considerably less than the vertical stress. The ratio of lateral effective stress to the vertical effective stress, termed the coefficient of earth pressure at rest, generally lies in the range 0.7-0,35, the lower values occurring in soils with a low plasticity index. The reduction in the value of cu/P which results when samples are consolidated in the laboratory under this stress ratio, instead of under equal all-round pressure, may be as much as 50%.
2) Reconsolidation in the laboratory after the disturbance which is associated even with the most careful sampling leads to a slightly lower void ratio than would occur in nature. The value of the pore-pressure parameter A in particular is sensitive to the resulting modification in soil structure an this, in turn, leads to a higher undrained strength - ($\Delta u=B(\Delta\sigma 3+A(\Delta\sigma 1-\Delta\sigma 3))$ -.

For these reasons the results of consolidated-undrained tests, expressed in terms of total stress, can be applied in practice only to a very limited extent. If the pore pressure is measured during the undrained stage of the test, the results can however be expressed in terms of effective stress. The values of c^1 and ϕ^1 thus obtained can be applied to a wider range of practical problems.

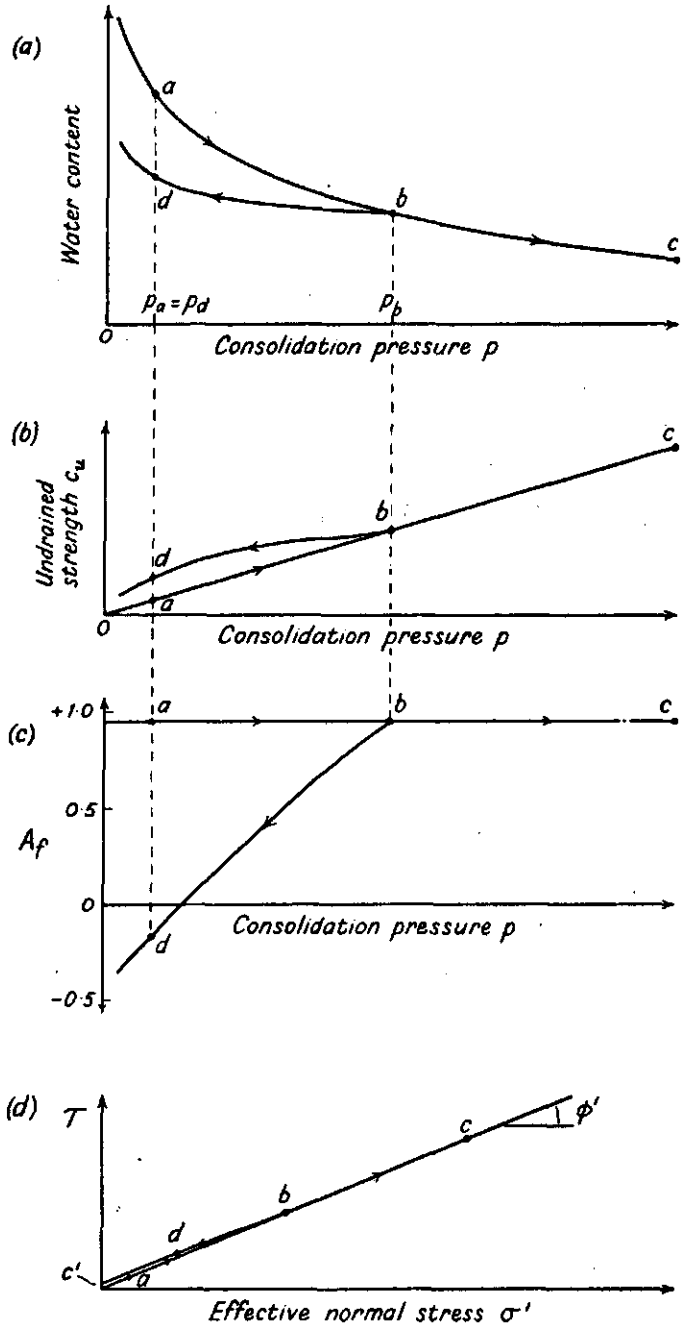

Fig. 3,19. Consolidated-undrained tests on saturated soil

(a) water content,

(b) undrained strength, and

(c) value of A_f, plotted against consolidation pressuere p;

(d) Mohr envelope in terms of effective stress.

In fig. 3.19 the relationships between the total stress, pore pressure and effective stress characteristics are illustrated. The points a, b and c represent normally consolidated samples; the point d represents an over-consolidated sample, the over-consolidation ratio being Pb/Pd (fig. 3.19(a)). For normally consolidated samples the effective stress envelope (fig. 3.19(d)) is a straight line with c^1 equal to zero, ϕ^1 depending on the type of soil. Over-consolidation results in an envelope lying a little above this straight line; a section of this envelope, over a specified stress range, being represented with sufficient accuracy by a slightly modified value of ϕ^1 and a cohesion intercept c^1.

The most marked effect of over-consolidation is, however, on the value of A, which, with increasing over-consolidation ratio, drops from a value typically about 1 at failure to values in the negative range.

These low A-values are, in turn, largely responsible for the high undrained strength values resulting from over-consolidation (compare point d, fig. 3.19(b), with point a). Values of c^1 and ϕ^1 are usually based on the effective stress circles corresponding to maximum deviator stress. In tests on over-consolidated clay samples and on samples of sand the limited values of c^1 and ϕ^1 may occur at an intermediate stage, as explained in the previous section. Here again the difference is of importance only in research investigations, a typical result for sands being an underestimate of ϕ^1 by about 2^o.

3.6.5. Consolidated-undrained test on partly saturated soils

This test may be called for in the determination of c^1 and ϕ^1 on undisturbed samples or on compacted samples of earth fill, in particular when the degree of saturation is not low enough to result in a sufficient range of strenghts in the undrained test to define a satisfactory failure envelope. It may also be used to examine the effect of c^1 and ϕ^1 of flooding foundation strata and earth-fill materials, and indicates the magnitude of the accompanying volume change.

Flooding, even for a period of months under an appreciable

hydraulic gradient, does not produce full saturation in the laboratory. Hence in all such tests the strength, measured during the undrained stage of the test, is not independent of changes in cell pressure at this stage, and cannot be expressed simply by a value of cu as in the case of a saturated soil. A total stress analysis is thus quite impractible. The values of the effective stresses at failure are obtained from measurement of the pore pressure and values of c^1 and ϕ^1 are thus determined.

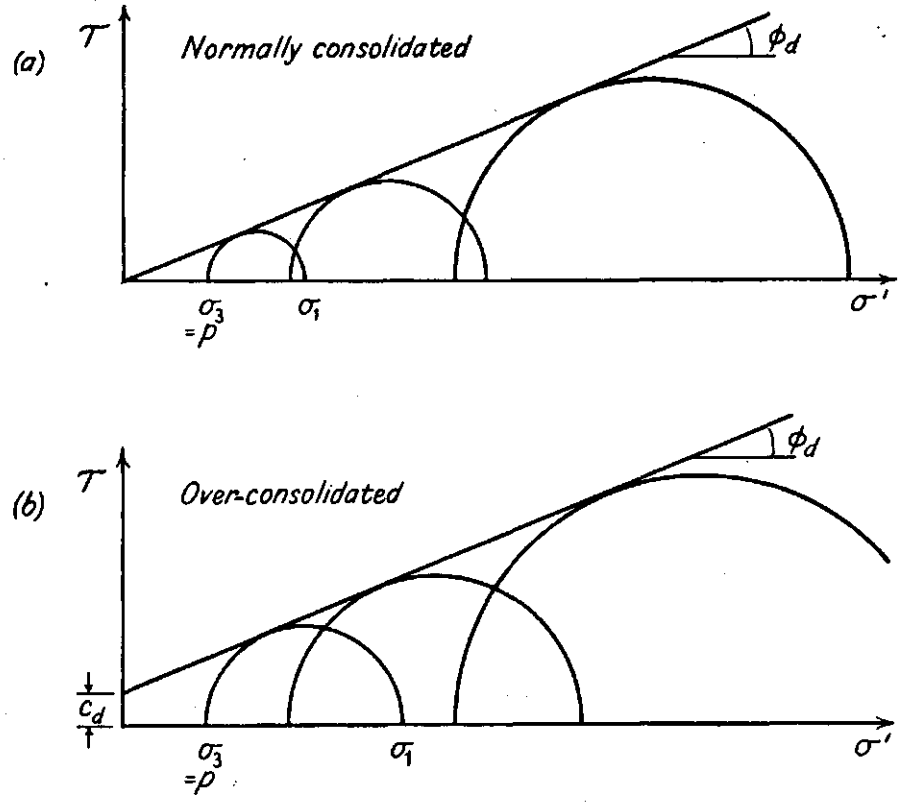

Fig. 3.20. Mohr stress circles for drained tests
(a) on normally consolidated samples, and
(b) on over-consolidated samples

3.6.6. Drained tests

Drained tests are carried out on soil samples of all types either undisturbed, remoulded, compacted or redeposited. The samples may be either fully or partly saturated. Cohesionless materials such as sand, gravel and rock-fill are often tested dry as it simplifies laboratory procedure. This may, however, lead to a slight over-estimate of the value of ϕ^1 in some cases. Tests on sugar, grain, etc., for silo design are also performed under normal "air-dried" conditions.

In the standard test consolidation takes place under an equal all-round pressure, and the sample is then sheared by increasing the axial load at a sufficiently slow rate to prevent any build-up of excess pore pressure. The minor principal stress σ_3^1 at failure is thus equal to p, the consolidation pressure; the major principal stress σ_1^1 is the axial stress. Since the pore pressure is zero, the effective stresses are equal to the applied stresses, and the strength envelope in terms of effective stress is obtained directly from the stress circles at failure, fig. 3.20. The values of c^1 and ϕ^1 obtained from drained tests are often denoted cd and ϕd respectively. The drained test also provides information on the volume changes which accompany the application of the all-round pressure and the deviator stress, and on the stress-strain characteristics of the soil.

3.6.7. General remarks on the interrelationship of the test results

1) For a given sample of soil the shear strength parameters c^1 and ϕ^1 are almost independent of the type of test used to measure them with the following qualifications:
   a) For normally consolidated clays the values of c^1 and ϕ^1 obtained from consolidated-undrained tests with pore-pressure measurement and from drained tests are, for practical purposes, identical provided comparable rates of testing are used.
   b) For heavily over-consolidated clays and for sands (except in a very loose state) the drained test will lead to slightly higher values of c^1 and ϕ^1, due to the work done by the increase in volume of the sample during shear and to the smaller strain at failure.

c) For some compacted fills and other partly saturated samples the value of c^1 will be reduced if an increase in water content occurs in the consolidated-undrained or drained test.

2) In contrast, deformation and volume-change characteristics in drained tests, and pore-pressure and undrained strength characteristics in consolidated-undrained tests, are largely controlled by the sequence and sign of the stress changes.

For practical purposes one should always simulate the stresses that occur in the soil under investigation and one has to decide whether the soil has to be studied under drained or undrained conditions.

3.7. Unconfined compression test

The unconfined compression test is in a sense a special form of triaxial test in which there is no horizontal pressure so the minor and intermediate principal stresses are zero. It is widely used in practice both in the field and for routine laboratory soil testing. It is used only on cohesive soils as such material does not require lateral support.

The in the test most commonly employed cylindrical sample is confined between end plates and loaded to failure by increase in axial pressure. Load has been applied by various means such as spring and hydraulic systems.

As in the triaxial test and unlike the direct shear test the failure surface is not pre-determined.

Failure may therefore occur in the weakest portion of the clay cylinder. The mid-portion of the sample is, however, subject to the greatest strain as the end portions are restrained laterally by the end plates.

If the sample fails in a brittle manner a definite maximum load before failure is recorded.

When plastic failure takes place no maximum load is reached and the strength at some arbitrarily defined strain such as 20% is taken in place of the peak.

LITERATURE TRIAXIAL TEST. Chapter 3.7.

BISHOP, ALAN W. and D.J. HENKEL, 1962. The measurements of soil properties in the triaxial test. Edward Arnold (publishers) L.T.D., London.

3.8. The different test procedures and their correlations

3.8.1. Correlations of cone resistance and vane shear strength for clays

LUNNE (1976) found a relationship between the cone factor N_k and the vane shear strength measured in scandinavian soft to medium stiff clays.

Terzaghi suggested the following formula

$$qc = N_k \sigma_f + \gamma.z.$$

where qc = cone resistance

N_k = cone factor

σf = undrained shear strength

γ = total unit wheight of soil

z = depth of penetration

After the application of the correction factor of Bjerrum for Scandinavian clays (see LUNNE, 1976) Lunne found a value of 15 to 19 for the N_k factor for soft to medium stiff clay with different plasticity (see fig. 3.21).

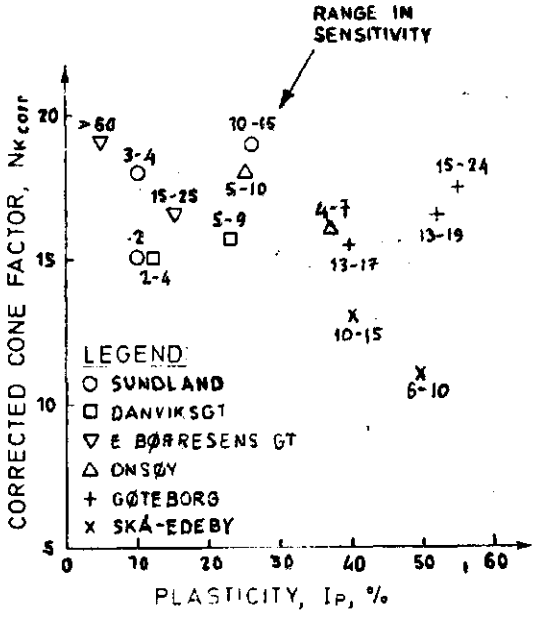

Plasticity = water content of soil between the plastic limit and liquid limt.

Fig. 3.21. Summary of corrected N_k values from all sites

3.8.2. Correlations of vane-test, unconfined compression test and undrained-unconsolidated triaxial test

Vane shear tests and shear annulus tests are used to determine the undrained shear strength of saturated or nearly saturated cohesive soils.

In principle one should find the same values for the shear strength as with the undrained-unconsolidated triaxial compression test.

MILLER (1966) found that the shear strength as obtained by triaxial methods was lower than by field and laboratory vane methods for samples tested to a depth of about 7,5 m, with close agreement below this depth (see fig. 3.22).

HALL (1963) reported that strengths determined by field vane tests were consistently higher than laboratory compression tests throughout the entire depth.

SIBLEY (1966) found that the correlation between the hand-operated torsional vane shear test results and those from unconfined and triaxial tests on saturated clays having shear strengths below 1 kg/cm^2 was very good (fig. 3.23).

SUDHINDRA and MELKOTE (1974) found for sensitive clays (sensitivity 5)* that the unconfined compression test gave significantly lower values as compared with either the deviator stress at failure in an unconsolidated undrained triaxial test or the field vane shear test results.

However the unconfined compression test was done in the field immediately after sampling, whereas the triaxial shear tests were done a few weeks later at the laboratory. The samples gain in strength after sampling.

VENEMAN (1976) found with the vane shear test somewhat higher values than with the unconfined compression test.

*The sensitivity of the clay is the ratio of the shear strength of an undisturbed sample to the remoulded strength. Clays have been subdivided into classes on the basis of their sensitivity as shown in table 3.2.

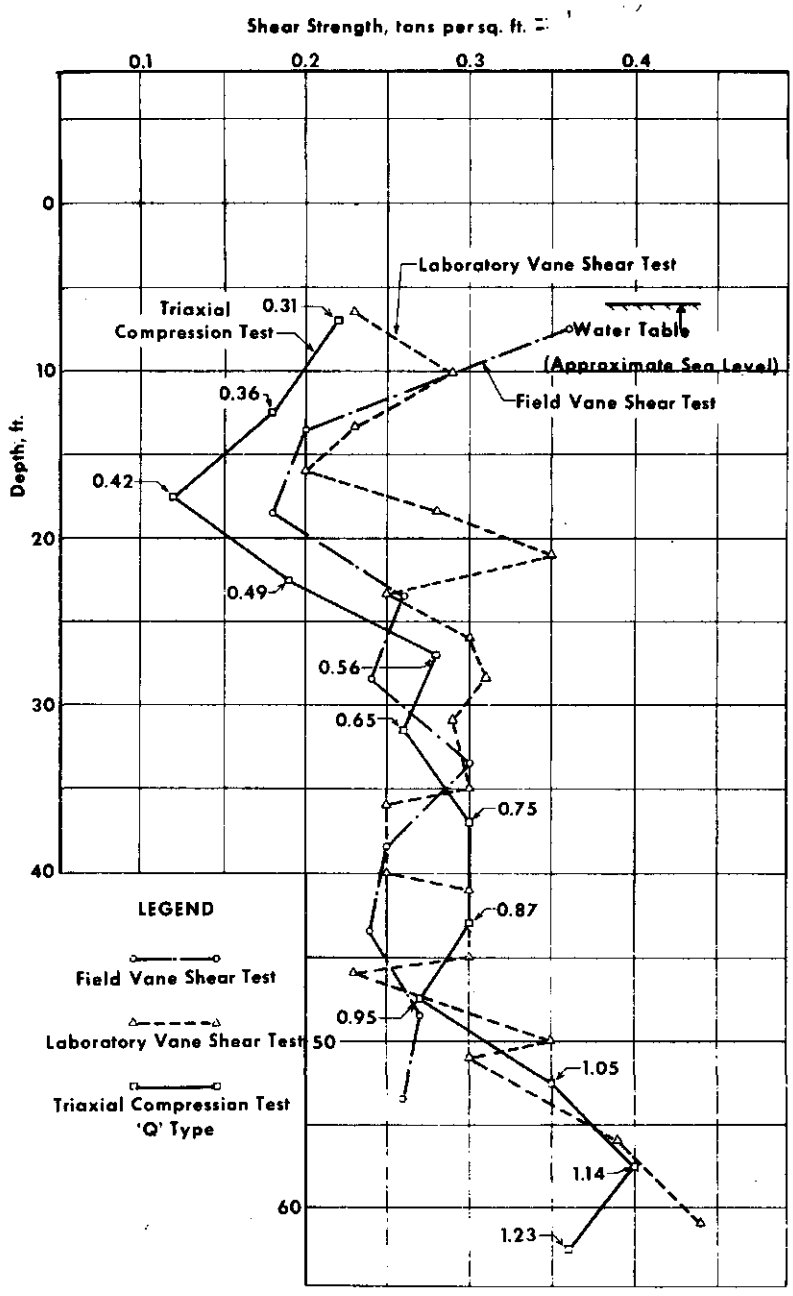

Fig. 3.22. Results of undrained shear tests by several methods on comparable soil. Laboratory vane shear results were taken from tests at "bit" end or bottom of each sample tube. (Number beside test point denotes confining pressure during test in tons per square foot). From MILLER (1966)

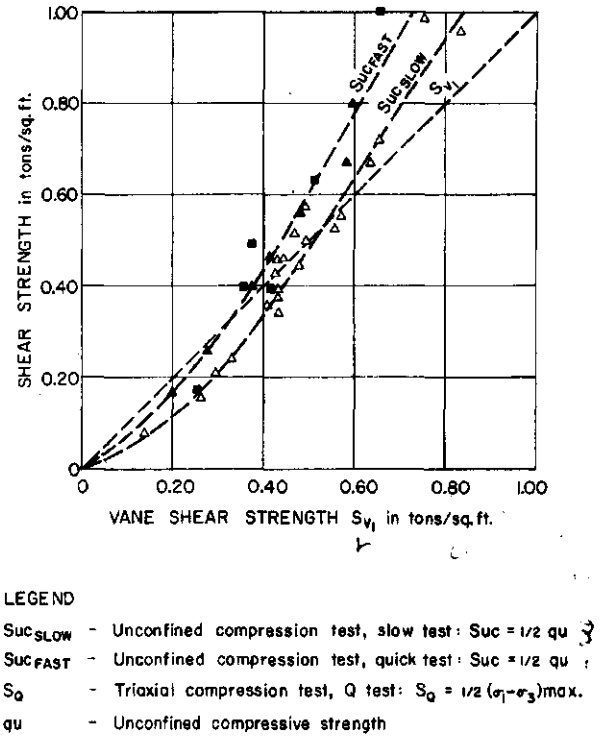

Fig. 3.23. Torsional vane shear strength relationship with other strength tests, Bootlegger Cove clay. From SIBLEY (1966)

Tabel 3.2. Classification of clay sensitivity[1] (after LEONARDS, 1962, p. 78)

Sensitivity	Classification
< 2	Insensitive
2-4	Moderately sensitive
4-8	Sensitive
8-16	Very sensitive
16-32	Slightly quick
32-64	Medium quick
>64	Quick

[1] Reproduced by permission of McGraw-Hill Book Company, Inc., New York, N.Y. From GILLOT, 1968

3.8.3. Correlations of cone index, triaxial test and vane test

W.E.S. (1964) stated the following relationship between the different measuring devices.

cone index = triaxial cohesion x 12,5 = vane shear strength x 10

for soils with a low shear strength and in which the friction angle is small $\phi < 4^{o}$

and

triaxial max. shear strength = vane shear strength + 0.6 psi

(see fig. 3.24 and 3.25).

The bevameter results given by the W.E.S. are too confusing and because this method is seldom used this measuring devise is not mentioned in this review.

LAMBE and WHITMAN (1969) give the following accuracy for the different test methods (tabel 3.3).

Table 3.3. Common Methods for Measuring Undrained Strength.
From LAMBE (1969)

Method	Comment
In-situ measurements	
1. Vane test	Usually considered to give best result, but is limited as to strength of soil with which it can be used
2. Penetration test	Gives crude correlation to strength
Measurements upon undisturbed samples	
1. Unconfined compression	Best general purpose test; underestimates strength because disturbance decreases effective stress
2. UU test at in situ confining pressure	Most representative of laboratory tests, because of compensating errors
3. CU test at in situ confining pressure	Overestimates strength, because disturbance leads to smaller water content upon reconsolidation

UU = unconfined undrained triaxial test

CU = confined undrained triaxial test.

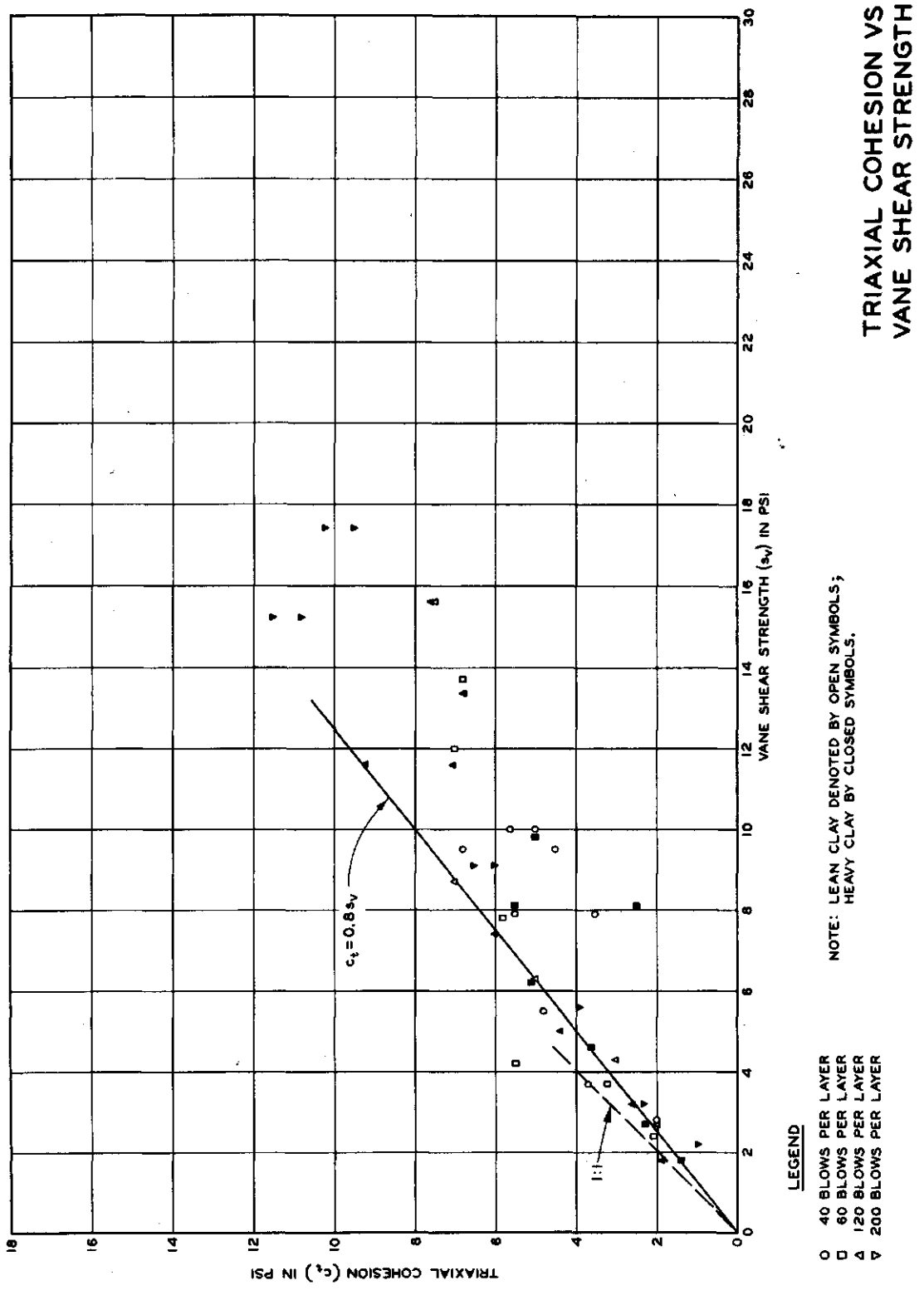

Fig. 3.24. From W.E.S. 1964

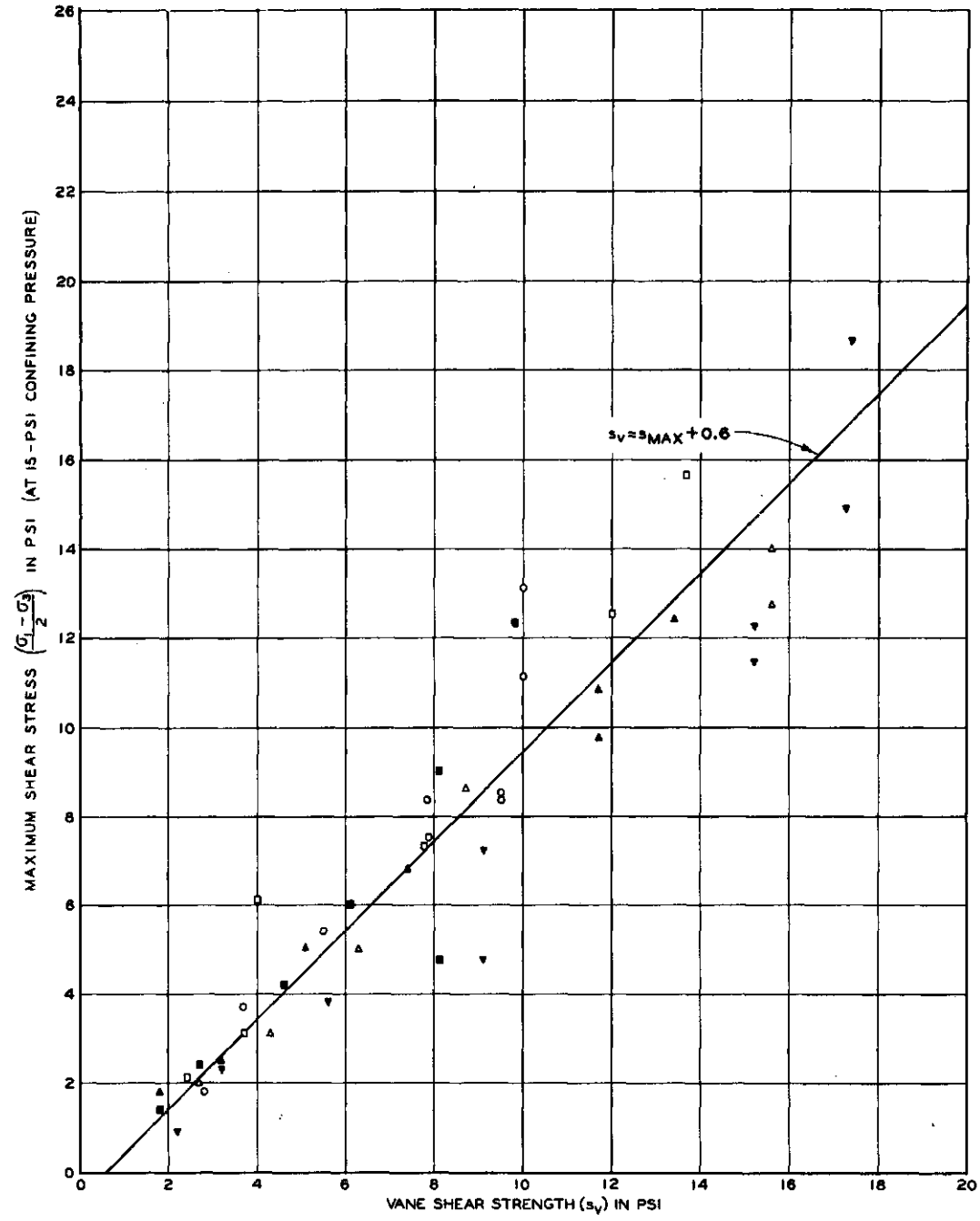

LEGEND

- ○ 40 BLOWS PER LAYER
- □ 60 BLOWS PER LAYER
- △ 120 BLOWS PER LAYER
- ▽ 200 BLOWS PER LAYER

NOTE: LEAN CLAY DENOTED BY OPEN SYMBOLS; HEAVY CLAY BY CLOSED SYMBOLS.

MAXIMUM TRIAXIAL SHEAR STRENGTH VS VANE SHEAR STRENGTH

Fig. 3.25. From W.E.S. (1964)

Because of sampling disturbance unconfined compression tests on even good quality samples usually somewhat underestimate the in-situ undrained strength, often by a factor of 2 or even more.

Use of the consolidated-undrained tests compensates for the effects of disturbance; indeed, such tests usually overestimate strength since the density of the soil increases during reconsolidation because disturbance has increased the compressibility of the mineral skeleton. The standard penetration test provides only a crude estimate of strength. Problems arise with the vane device because of disturbances as the device is inserted into the ground, rate-of-strain etc.

It generally (but not always) has been found that properly conducted vane tests and unconfined compression tests upon good undisturbed samples give strengths which are within 25%. The vane test usually, but not always, gives a larger strength for a given soil than does the unconfined compression test.

In short, because the undrained strength of a soil is somewhat sensitive to test conditions, it is difficult to establish undrained strength within about 20% at best.

3.8.4. Comparison of methods of measuring soil shear strength using artificial soils. BAILEY (1965)

Comparison of triaxial test, sheargraph, torsion head annular grouser plate, enclosed annular grouser plate using an artificial soil. For results see fig. 3.26 and 3.27.
Sheargraph = loaded shear annulus or shear vane with automatically registration.

The artificial soil (1) was similar to a sandy loam and the artificial soil (2) was a clayey and compressible soil with sensitivity 10.

From the study Bailey concluded that the assumption of a uniform stress distribution across the head of the sheargraph would be more accurate than the linear distribution which are used for peak shearing-stress calculations.

General agreement in the measurement of shear strength was found between the sheargraph and the torsional shearhead. Side effects on

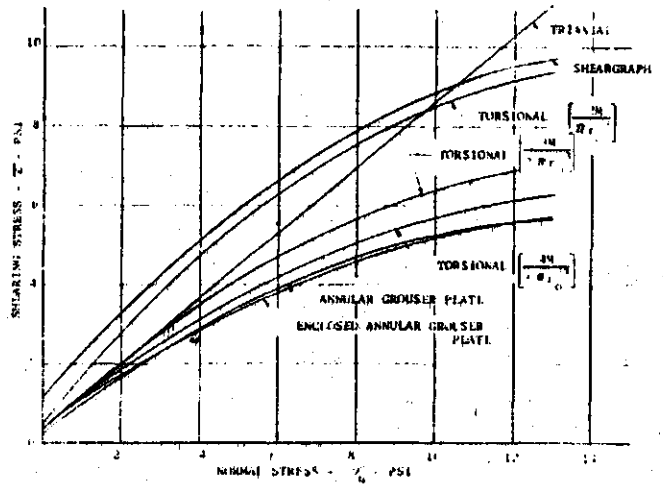

Fig. 3.26. Coulomb failure envelopes for soil 1. From BAILEY (1965)

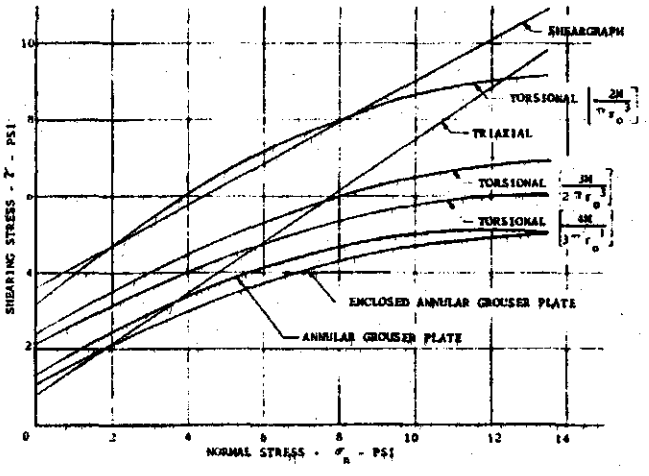

Fig. 3.27. Coulomb failure envelopes for soil 2. From BAILEY (1965)

the annulus were found to be negligable. Strength values indicated by the torsional shearhead were always higher than those from the annulus.

There was also an indication that the differences in results among the various devices varied with the soil being used.

Table 3.4. Schematic review of test correlations and literature cited

	static penetrometer	dynamic penetrometer	vane test	shear annulus	solid shearhead	direct shear test	triaxial test	unconf. compr. test	actual undrained shear strength
static penetrometer			LUNNE, 1976 good agreement W.E.S., 1964 good agreement				W.E.S., 1964 good agreement		crude estimate
dynamic penetrometer								LAMBE	
vane test					BAILEY, 1975 good agreement		W.E.S., 1964 good agreement MILLER, 1966 UU<vane test d<7,5 m UU=vane test d>7,5 m HALL, 1963 ref. Miller UU<vane test at any depth	SIBLEY, 1966 good agreement SUDHINDRA, 1974 U.Conf. < vane LAMBE+WHITMAN, 1969 U.C.=Van + (-) 25%	best result
shear annulus					BAILEY, 1965 shearhead >annulus				
solid shearhead									
direct shear test									
triaxial test U.U. C.U.								SIBLEY, 1966 good agreement SUDHINDRA, 1974 unconf. < triax.	most repres. of lab. test overestimate
unconfined compression test									underestimate sometimes factor 2

LITERATURE CHAPTER 3.8.

BAILEY, A.C. and J.A. WEBER, 1965. Comparison of Methods of Measuring soil shear strength using artificial soils. Transactions of the ASAE vol. 8, no. 2, p. 153.

GILLOT, J.E., 1968. Clay in engineering geology. Elsevier Publishing Company, Amsterdam.

LAMBE, T. WILLIAM and ROBERT V. WHITMAN, 1969. Soil Mechanics. Massachusetts Institute of Technology John Wiley and Sons, Inc. New York, London, Sydney.

LUNNE, T., O. EIDE and J. DE RUITER, 1976. Correlations between cone resistance and vane shear strength in some Scandinavian soft to medium stiff clays. Can. Geotech. J. 13, 430.

MILLER, E.A. and E.B. HALL, 1966. A comparison of soil shear strenghts as determined with field and laboratory vane shear apparatus. Vane shear and cone penetration resistance testing of in-situ soils, ASTM STP 399, Am. Soc. Testing Mats. p. 18.

SIBLEY, E.A. and G. YAMANE, 1966. A simple shear test for saturated cohesive soils. Vane shear and cone penetration resistance testing of in-situ soils. ASTM STP 399, Am. Soc. Testing Mats. p. 39.

SUDHINDRA, C. and R.S. MELKOTE, 1974. Some experiences in evaluation of undrained shear strength of saturated sensitive clays. Irrigation and power, vol. 31, no. 4, october.

VENEMAN, P.L.M., J. BOUWMA and T.B. EDIL, 1976. Soil shear strength variation in soils of a Batavia Silt loam mapping unit. Soil Sci. Soc. Am. J. vol. 40, pp. 462-465.

W.E.S., 1964. Strength-moisture-density relations of fine-grained soils in vehicle mobility research, Technical report no. 3-639 January. U.S. Army Engineer Waterways Experiment Station Corps of Engineers. Vicksburg, Mississippi.

4. FRICTION ANGLE AND SHEAR STRENGTH OF COHESIONLESS SOILS

4.1. Definition of friction angle

Two alternative ways of expressing frictional resistance are in common use. The first is to use the coefficient of friction ϕ. Thus, if N is the normal force across a surface the maximum shear force on this surface is Tmax = Nf.

The second is to use a friction angle $\phi\mu$ defined such that $\tan \phi\mu = f$. $\phi\mu$ is particle to particle friction, whereas ϕ is the analytical friction angle of the Coulomb-Mohr equation.

The geometric interpretation of $\phi\mu$ is shown in fig. 4.1.

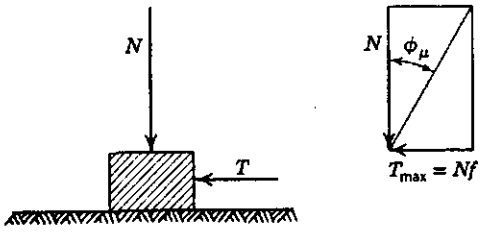

Fig. 4.1. Definition of friction angle $\phi\mu$. From LAMBE, 1969

4.2. Friction between minerals in granular form

The particles of coarse silt have a minimum diameter of 0,002 cm (20 μ or 2000 0000 A^o). The diameters of these and larger particles are clearly larger than the height of the asperities (about 1000 - 10 000 A^o) that may be expected on the surfaces of these particles.

Consequently we would expect that each apparent point of contact between particles actually involves many minute contacts.

The surfaces of these soil particles are of course contaminated with water molecules and various ions and possibly other materials. These contaminants are largely squeezed out from between the actual points of contact, although some small quantity of contaminants

remains to influence the shear strength of the junctions.

The minimum diameter of fine silt particles is 2 μ or 20 000 A^{o}. Such small particles have dimensions of the same order as the height of the asperities on larger particles. For these small particles it makes more sense to talk about "corners" rather than asperities. Although the general nature of the frictional resistance is the same for either large or small granular particles, an apparent contact between very small granular particles may, in fact, consist of only one actual contact point.

The testing systems shown in fig. 4.2. have been used to determine the frictional resistance for minerals. When fixed buttons on sliding blocks are used (fig. 4.2.) the results give the static (and perhaps kinetic) coefficient of friction. When many sand particles are pulled over a flat surface (fig. 4.2.) the results generally reflect some combination of sliding and rolling friction. Hence the friction factor as measured by the second type of test involving many particles may be different from the value measured by the first type of test.

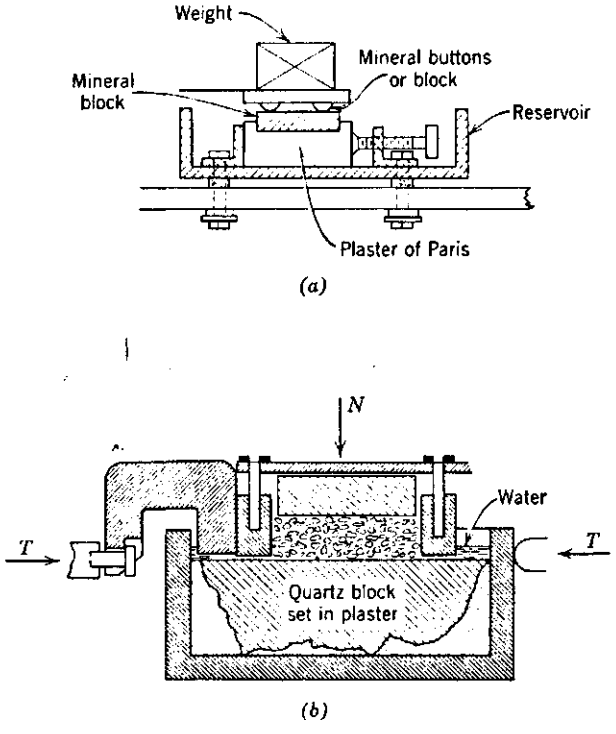

Fig. 4.2. Devices for measuring friction factor of mineral surfaces. (a) Sliding on buttons or on block. (b) Sliding of many particles

4.3. Effect of surface water and surface roughness

Fig. 4.3. summarizes the friction factors observed for quartz under varying conditions of surface clearliness, humidity, and surface roughness.

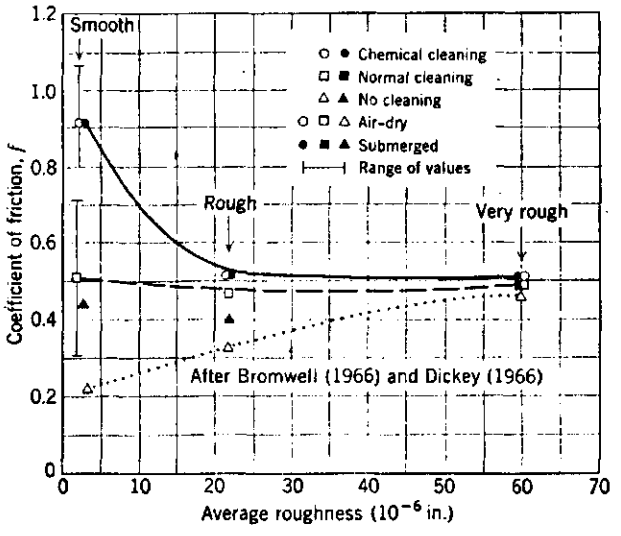

Fig. 4.3. Friction of quartz (after BROMWELL (1966) and DICKEY (1966). From LAMBE (1969)

The results show that the friction of smooth quartz varies from about f = 0.2 to f = 1.0 depending on the surface cleanliness.

For the more contaminated surfaces water increases the friction; i.e. it acts as an antilubricant. However, for carefully cleaned surfaces, water has no effect.

But if there is a contaminating layer (probably a thin film of organic material) the water disrupts this layer, reduces its effectiveness as a lubricant, and thereby increases the friction. As the surfaces get rougher the effects of cleaning procedure on friction decrease, so that a very rough surface of 60 μ in. (about 15 000 A^{o}) gives essentially the same value of f independent of surface cleanliness. This indicates that the ability of the contaminating layer

to lubricate the surfaces decreases as the surface roughness increases. This is what we would expect from a thin lubricating layer which acts as a boundary lubricant.

The fact that the rougher surfaces do not give higher values of friction when they are carefully cleaned is more difficult to explain.

The evidence seems to indicate that the rougher surfaces cannot be cleaned as effectively as smooth surfaces, although the reason for this is not clear.

From a practical point of view the essentially constant value of f = 0.5 ($\phi\mu = 26^{o}$) for very rough quartz surfaces is of great significance, since essentially all quartz particles in natural soils have rough surfaces.

Values of friction for other nonsheet minerals are summarize- in table 4.1.

Table 4.1. Friction of Nonsheet Minerals. From LAMBE, 1969

	Conditions of Surface Moisture			
Mineral	Oven-Dried	Oven-Dried; Air-Equilibrated	Saturated	ϕ
Quartz[a]	0.13	0.13	0.45 =	$21,2^{o}$
Feldspar	0.12	0.12	0.77 =	$37,6^{o}$
Calcite	0.14	0.14	0.68 =	$34,2^{o}$

The low values of f for these minerals in the air-day condition probably have no practical significance, since they represent ineffective cleaning of smooth, polished surfaces. Much more data are needed for these other minerals before one can confidently choose f values.

FEBENE and DE BOODT (1970) gave the values for the internal friction angle of Bredene sand with varying moisture content (fig. 4.4.).

There was little influence of the moisture content on the friction angle.

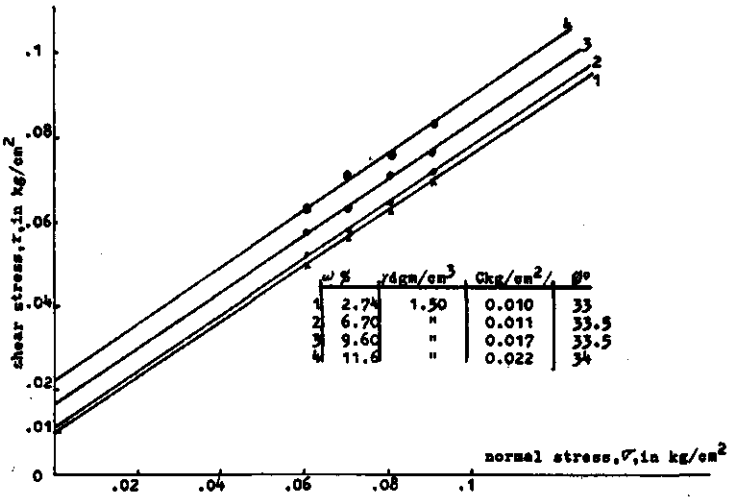

Fig. 4.4. Shear parameters at different moisture contents. From FEBENE (1970)

The mechanical analyses of the sand was as follows

fraction	%
< 2 μ	2.5
2-50 μ	5.7
>50 μ	91.7

The measurements were taken with the shearbox.

ZEITLER (1966) found also that water had little influence on the internal friction angle (fig. 4.5.) Sand used was fine dune sand 0.16 mm < D50 > 0.22 mm, the test method was the shearbox.

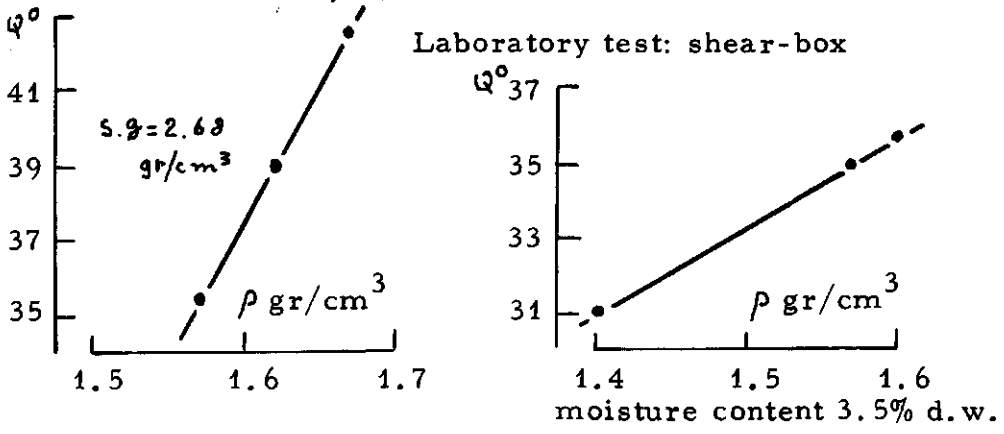

Fig. 4.5. Sand oven-dried. From ZEITLER (1966)

4.4. Effect of normal load

The measured friction factors for nonsheet minerals have been found to be independent of normal load. Based on tests in which the normal load per contact varied by a factor of 50, ROWE (1962) reported that the friction angle of $\phi\mu$ remained constant within $\pm$ 1° (see LAMBE (1969)).

$\phi\mu$ is the interparticle friction.

On the other hand, Rowe's results show that the friction angle ϕu is affected by the size of the particle involved in the test (fig. 4.6.).

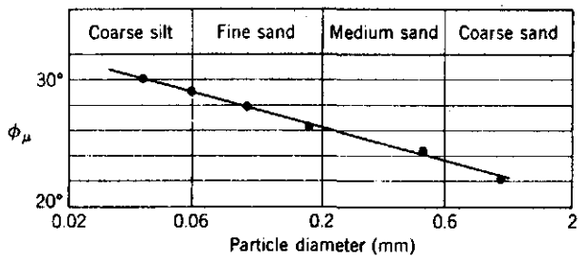

Fig. 4.6. Friction angle of quartz sands as function of grain size (after ROWE, 1962). From LAMBE (1969)

Rowe used the test procedure shown in fig. 4.2(b). For a given total normal load the normal load per contact increases as the particle size increases. However, since the particle diameter in this case also increases, the average contact stress did not change. Therefore arguments involving elastic deformation do not appear adequate to explain these data. One possible explanation is that the larger particles are able to roll more easily than the smaller particles, perhaps as a result of their center of gravity being further away from the plane of shear. Hence the measured friction angle which involves both rolling and sliding components is smaller for the larger particles.

4.5. Effect of confining stress on the shear strength

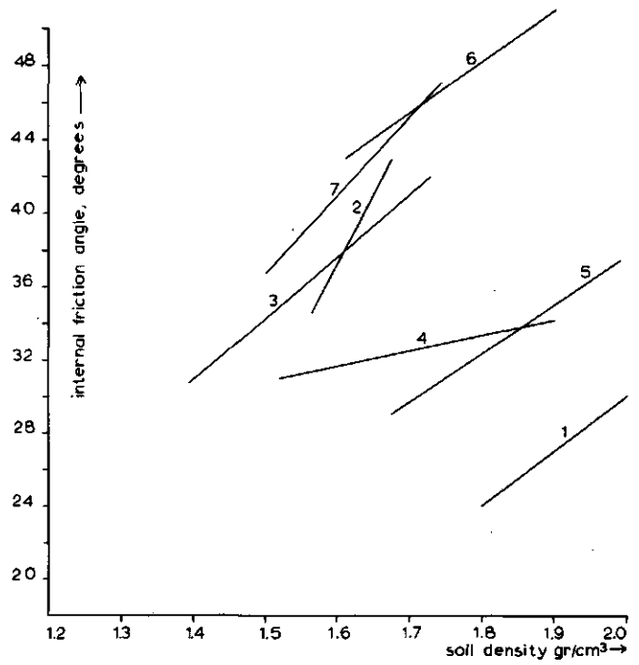

Fig. 4.9. Relation between density and friction angle of different sands

Table 4.2. Origin of the data from fig. 4.9

	particle size distribution	test method	author
1. Fine sand	0,105-0,21 mm	triaxial test consolidated undrained	Heidemij 1976
2. Fine dune sand	0,125-0,26 mm	direct shear test drained	Zeitler 1966
3. Fine dune sand	0,16 mm D50 < 0,22 mm	direct shear test drained	Wiseman 1962
4. Bredener sand	2,5% < 0,002 mm 5,7% (0,002-0,05 mm) 91,7% >0,05 mm	direct shear	Febere 1970
5. Friese woudgrond	fijn zand	celproef	Huisman 1969
6. Duinzand		celproef	Huisman 1969
7. Rivierzand		celproef	Huisman 1969

Fig. 4.10 gives some values of the internal friction angle for different sands with varying porosity.

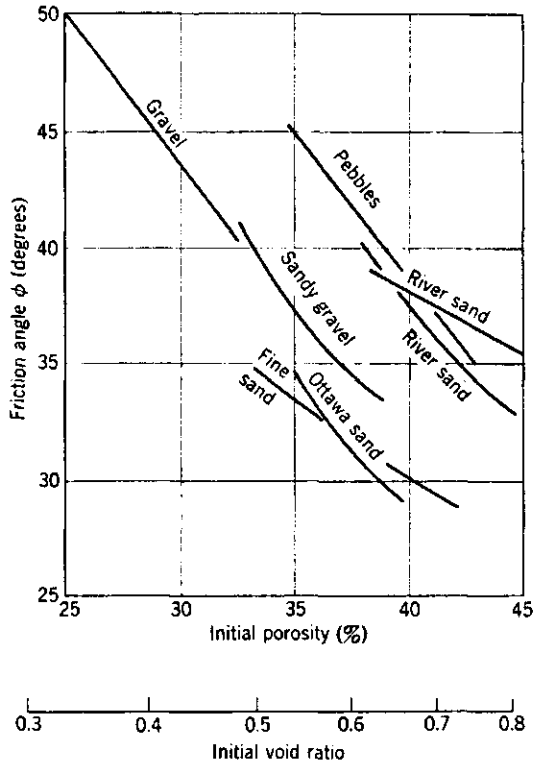

Fig. 4.10. Friction angle versus initial porosity for several granular soils

4.7. R a t e o f l o a d i n g

The friction angle of sand, as measured in triaxial compression, is substantially the same whether the sand is loaded to failure in 5 millisec or 5 min. The increase in tan ϕ from the slower to the faster loading rate is at most 10%, and probably is only 1-2%. It is possible that the effect might be somewhat greater if the confining pressure is in excess of 100 psi (WHITMAN and HEALY, 1963 (see Lambe and Whitman)).

4.8. Vibrations and repeated loadings

Repeated loadings, whether changing slowly or quickly, can cause ϕ to change. A loose sand will densify, with resulting strength increase, and a dense sand can expand, with resulting strength decrease.

A stress smaller than the static failure stress can cause very large strains if the load is applied repeatedly (SEED and CHAN, 1961), see LAMBE, 1969.

4.9. Average particle size

Fig. 4.11 shows data for five soils all having a uniformity coefficient of 3.3 but having different average particle sizes. For a given compactive effort, these sands achieve different void ratios, e_o, however, the friction angle was much the same for each sand. The effect of the greater initial interlocking in the sand with the largest particles is compensated by the greater degree of grain crushing and fracturing that occurs with the larger particles because of the greater force per contact.

Crushing of particles and the consequent curvature of the Mohr envelope is most important with large particles, especially gravel-sized particles or rock fragments used for rockfills. This is because increasing the particle size increases the load per particle, and hence crushing begins at a smaller confining stress.

4.10. Determination of in-situ friction angle

The results presented in the foregoing sections have emphasized the predominant role of the degree of interlocking upon magnitude of the friction angle. Thus, if we wish to determine the friction angle of a sand in-situ, it is not enough to find the nature and shape of the particles composing the sand. It is essential to know how tightly together these particles are packed in their natural state. It is extremely difficult to obtain samples of a sand without changing the porosity. Thus, except for problems involving man-made fills, it is difficult to either measure or estimate the friction

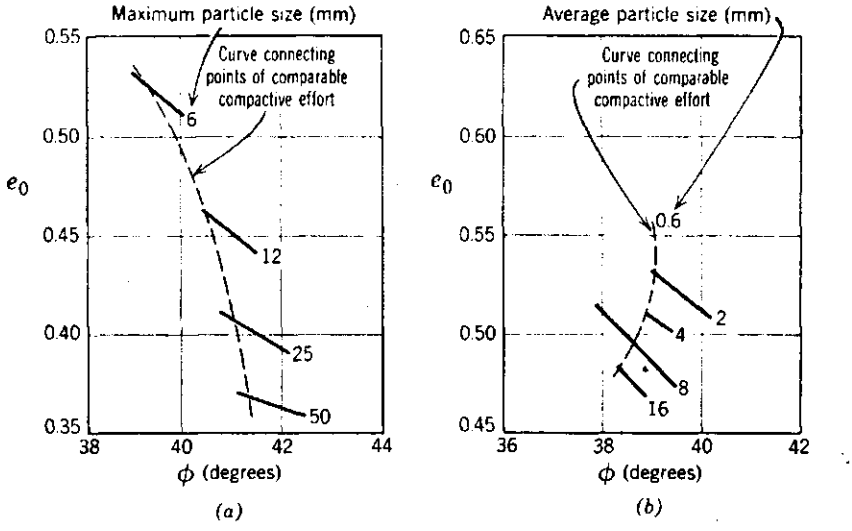

Fig. 4.11. Effect of particle size and gradation on friction angle. (a) Soils with same minimum particle size. (b) Soils with same uniformity coefficient. Data from LESLIE (1963). From LAMBE, 1969

angle of a sand on the basis of laboratory tests alone.

For these reasons extensive use is made in practice of correlations between the friction angle of a sand and the resistance of the natural sand deposit to penetration (see penetration spoon).

Other in-situ measurement of the friction angle is possible with the direct shearbox.

4.11. Summary. The choice of friction angle values for preliminary calculations

1) The shear resistance is determined primarily by the magnitude of the current normal load, so that the overall behavior is frictional in nature.
2) For quartz the friction angle $\phi\mu$ is generally in the range of 26° to 30°. Because the surfaces of such particles are rough the presence or absence of water has little or no effect on the frictional resistance.

3) The strength of soil can be represented by a Mohr envelope. Generally the Mohr envelope of a granular soil is curved. For stresses less than 100 psi, the envelope usually is almost straight so that

$$\tau = \sigma \tan \phi$$

where ϕ is the friction angle corresponding to the peak point of the stress-strain curve.

The value of ϕ for any soil depends upon $\phi\mu$ and upon the amount of interlocking; i.e. the initial void ratio (or density) and the loads applied to the soil.

Where sand is being subjected to very large strains ϕcv should be used in the failure law.

Unless the sand is very loose ϕcv will be less than ϕ. Where the sand is sliding over the surface of a structure the friction angle will vary from $\phi\mu$ to ϕcv depending on the smoothness of the surface.

Tabel 4.3. Summary of friction angle data for use in preliminary design

	Friction Angles					
	At Ultimate Strength		At Peak Strength			
			Medium Dense		Dense	
Classification	$\phi_{cv}(^o)$	$\tan \phi_{cv}$	$\phi(^o)$	$\tan \phi$	$\phi(^o)$	$\tan \phi$
Silt (nonplastic)	26 to 30	0.488 to 0.577	28 to 32	0.532 to 0.625	30 to 34	0.577 to 0.675
Uniform fine to medium sand	26 to 30	0.488 to 0.577	30 to 34	0.577 to 0.675	32 to 36	0.675 to 0.726
Well-graded sand	30 to 34	0.577 to 0.675	34 to 40	0.675 to 0.839	38 to 46	0.839 to 1.030
Sand and gravel	32 to 36	0.625 to 0.726	36 to 42	0.726 to 0.900	40 to 48	0.900 to 1.110

From LANBE and WHITMAN, 1969. cv = constant volume

LITERATURE ON FRICTION ANGLE AND SHEAR STRENGTH OF CHAPTER 4. COHESIONLESS SOILS.

FEBERE, A.E. and M. DE BOODT, 1970. Comparative study of the improvement of the angle of internal friction and cohesion in sand using different stabilizing agents. Pedologie-Bulletin de la Société Belge de Pédologie. Vol. 20, no. 1.

HEIDEMIJ, 1976. Bodemkundig-grondmechanisch rapport. Rapport nr. 667-76/3. Hoofdwatergangen in de ruilverkaveling Voorne-Putten. Dienst voor de landinrichting in Zuid-Holland.

HUISMAN, ir. T.K., 1969. Grondmechanica. Agon Elsevier, Amsterdam/ Brussel.

KHOSLA, VIJAY K. and TIEN H. WU, 1976. Stress-Strain Behavior of sand. Journal of the Geotechnical engincering division. G.T. 4 april.

LAMBE, T. WILLIAM and ROBERT V. WHITMAN, 1969. Soil mechanics. Massachusetts Institute of Technology John Wiley and Sons. Inc. - New York.

WISEMAN, G., 1962. Laboratory soil engineering studies on dune sand. Technion-Israel Institute of Technology. Faculty of civil engineering. Haifa, Israel. Publication no. 20.

ZEITLER, JOSEPH G. and Y. NEGRI, 1966. Study of horizontal and vertical loading tests on a sand. Technion-Israel Institute of Technology. Faculty of civil engineering. Publication no. 31.

5. FRICTION ANGLE, COHESION AND SHEAR STRENGTH OF COHESIVE SOILS

5.1. Friction between sheet minerals

5.1.1. General nature of contact

Surfaces of mica do show irregularities, but in the form of mesas and plateaus rather than in the form of asperities. Moreover, the scale of these irregularities is quite different from that existing in the surfaces of granular particles. On fresh cleavage surfaces the "steps" are only as high as the thickness of several repeating sheet units (about 10-100 A^{o}),

In the words of BOWDEN and TABOR (1964), see LAMBE, 1969, the cleavage surfaces are molecularly smooth over large areas". Compared to the surfaces of smooth quartz particles, fresh cleavage surfaces are "supersmooth". There are reasons to believe that the surfaces of clay particles are similar. Unfortunately the fundamentals of frictional resistance between supersmooth surfaces have received relatively little study and hence the following explanations are still largely speculative.

Two cleavage faces of mica give quite a different contact than do surface with asperities. Mica, and presumably clay, surfaces should come into close proximity over almost their entire area, but they may not actually come into direct contact. The contaminants on the surfaces, including adsorbed water, are not squeezed out from between the surfaces, unless the normal stress exceeds about 5625 kg/cm^2. Rather, these contaminants participate in the transmission of the normal stress.

A more normal situation for clay particles is probably some sort of edge-to-face orientation. This type of contact is more nearly similar to the asperity contacts discussed for granular particles, except that in the case of clays each contact probably consists of only one 'asperity".

It still remains to discuss whether the shear resistance between very smooth surfaces is greater or less than the resistance between rough surfaces. To answer this we must turn to experimental data.

5.1.2. Effect of soil moisture content on the friction angle

The data in table 5.1 show that the water acts as a lubricant.

Table 5.1. Friction factors for several-layer lattice materials under varying conditions of humidity

	Condition of Surface Moisture		
Mineral	Oven-Dried	Oven-Dried; Air-Equilibrated	Saturated
Muscovite mica	0.43	0.30	0.23
Phlogopite mica	0.31	0.25	0.15
Biotite mica	0.31	0.26	0.13
Chlorite	0.53	0.35	0.22

Notes. Starting and moving friction identical. Data from HORN AND DEERE (1962). Friction factor = tan ϕ. (From LAMBE, 1969)

A possible explanation for this behavior is as follows. In the oven-dried condition the surface ions are not completely hydrated. The actual mineral surfaces come close together and the binding is strong. As water is introduced the ions hydrate and become less strongly attached to the mineral surfaces. Hence the shear resistance drops as water is introduced.

It is important to contrast the role of the contaminants for the cases of very smooth and rough surfaces. With rough surfaces the contaminants serve to weaken the crystalline bond, and increasing the mobility of the contaminants with water helps to get them out of the way and hence minimizes their adverse influence. With very smooth surfaces the contaminants are actually part of the mineral, and increasing their mobility decreases the shear resistance.

In the saturated condition the friction angle between sheet minerals can be low. Since clay minerals are always surrounded by water in practical situations it is important to test these minerals in the saturated condition.

Few data are available about the relation between moisture content and friction angle of clayey soils.

Fig. 5.1 shows this relationship for a heavy clay, percentage 2 μ > 47%.

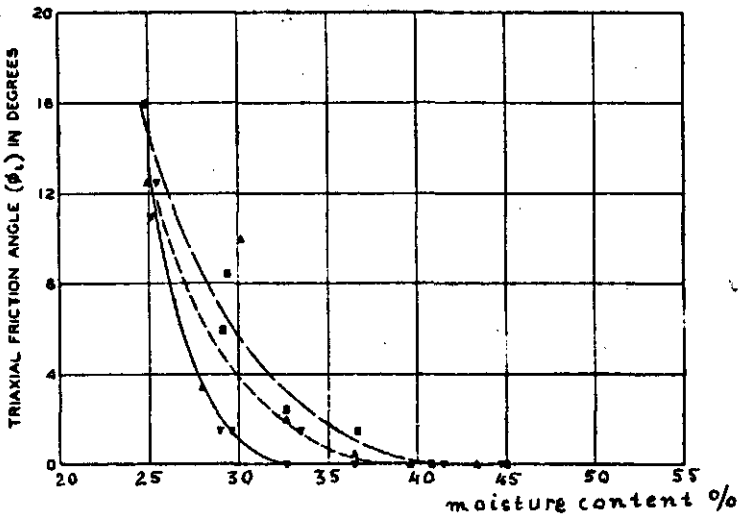

Fig. 5.1. Relation triaxial friction and moisture content. The three different lines represent different soil densities. From W.E.S. (1964)

For the heavy clay soils ϕ is supposed to be negligable at the point of saturation, so the shear strength at that point is entirely due to the cohesion which can be measured with the vane apparatus.

VAMOCIL and CHANCELLOR (1967) have found for three agricultural soils the following relationship between friction angle and moisture content (see fig. 5.2 and table 5.2).

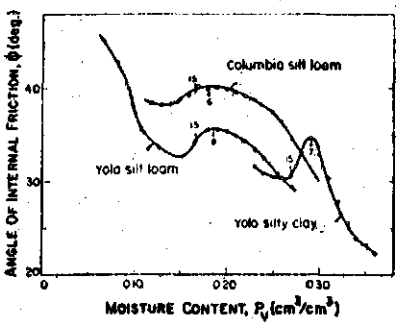

Fig. 5.2. Covariation of angle of internal friction, ϕ (based on the frictional model), with volume fraction moisture content. (The numbers with arrows along the curves correspond to the soil moisture suctions at the indicated moisture contents). From VOMOCIL (1967)

Table 5.2. Characteristics of soils used in strength tests[o]

	Yolo silt loam	Yolo silty clay	Columbia silt loam
Sand	34.2	10.6	53.2
Silt	49.2	48.0	41.5
Clay	16.6	41.4	5.3
Liquid limit	33.1	47.1	...,.†
Lower plastic limit	20.3	21.6	....†
1/3-bar moisture	21.4	32.9	22.7
15-bar moisture	11.3	17.9	11.6

[o]All table entries are percentage by weight. † Nonplastic.
From VOMOCIL (1967)

The test procedure used here was the unconfined compression test. Fig. 5.2 indicates a maximum value for ϕ at a moisture suction in the range of 6-8 bar ($\pm$ P.F. 3.8). Further the figure shows a decrease in the value for ϕ with increasing clay content.

5.1.3. Effect of soil density on the friction angle

There is a good evidence that a higher soil density always gives a higher value for the friction angle of a soil (see fig. 5.3).

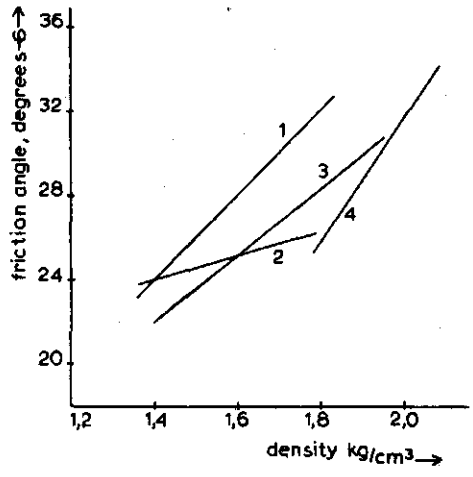

Fig. 5.3. Relationship between internal friction angle and density for different soils

Table 5.3.

1 - sandy clay loam	% < 2μ 25-35
2 - loam	18-25
3 - silt loam	5-18
4 - stiff clay	liquid limit 80% moisture plastic limit 30% moisture

The data 1 to 3 are from HEIDEMIJ, 1976 and are the results of saturated undrained-consolidated undisturbed samples.

The data for curve 4 come from MIRATA, 1974, which are obtained from measurements with the slow shear box.

5.1.4. Correlation of drained friction angle and particle size distribution

HUMPHREYS (1975) has tried to find a relationship between the internal friction angle and the particle size distribution of the soil. He found the following relationship

$$j = a + 2\left(\frac{b-a}{\sqrt{a}}\right)$$

where j = internal friction angle

a = percentage smaller than 0.002 mm

b = percentage smaller than 0.02 mm (see fig. 5.3.)

This relation gives a better correlation than the graph of Kainji who tried to find a relationship between the friction angle and plasticity index (see next chapter 5.3).

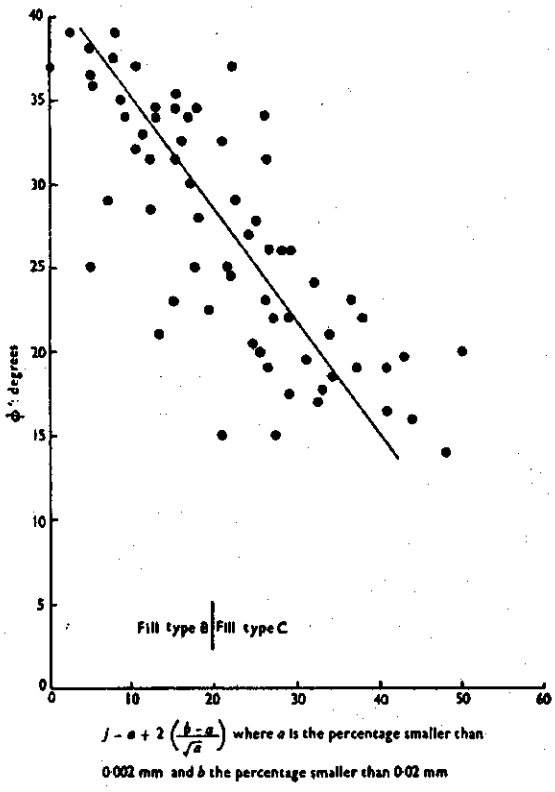

Fig. 5.3. Values of ϕ and j for samples from Kainji dam, Nigeria. From HUMPHREYS (1975)

5.1.5. Correlation of drained friction angle and plasticity index

KAINJI (1974) proposed the following expression for the relation between plasticity index and the friction angle measured at residual strength

$$\phi = 46.6/I_p^{0,446}$$

where ϕ = drained angle of internal friction

I_p = plasticity index, here from 5 to 50%

He found this relation from measurements of his own and that of others (see fig. 5.4).

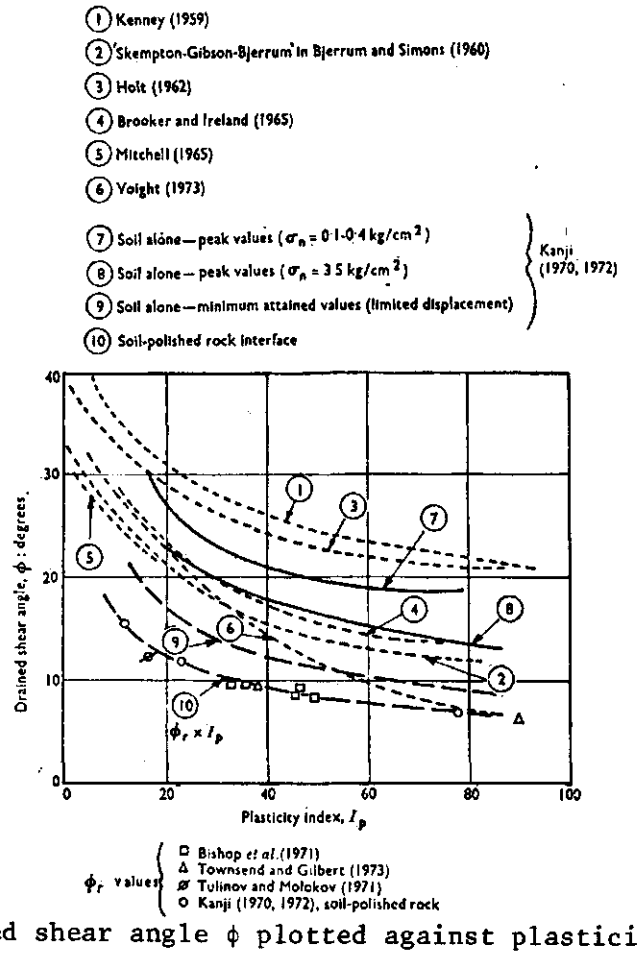

Fig. 5.4. Drained shear angle ϕ plotted against plasticity index I_p
From KAINJI (1974)

Plasticity index is the moisture content between the liquid limit and the plastic limit, here in percentage of dry weight.

5.2. Cohesion of clay soils

5.2.1. Cohesion and moisture content

Cohesion is taken here as the intercept of the Mohr-Coulomb failure envelope with the shear-strength axis in the shear strength normal load plot.

Fig. 5.5 shows the relation between cohesion as measured with the triaxial test and the moisture content (see also table 5.4). There is a good evidence that cohesion decreases with increasing moisture content. The heavy clays have higher cohesion values than the more sandy clays at the same moisture content.

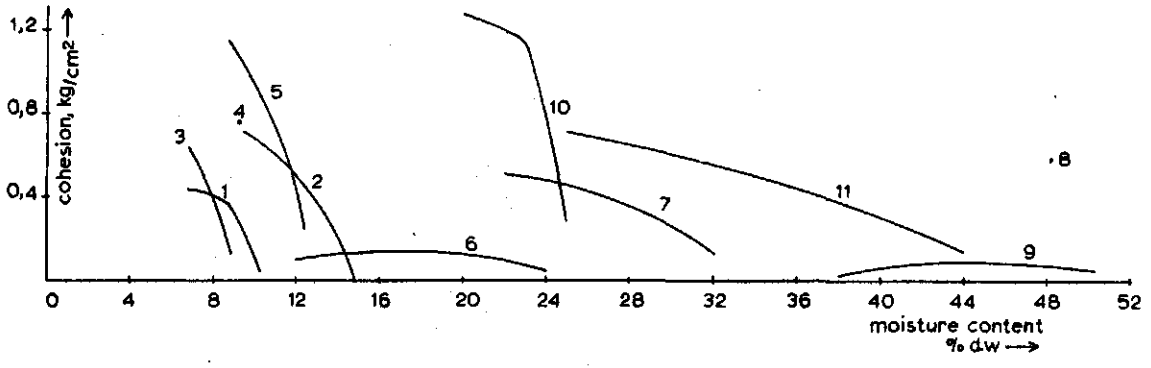

Fig. 5.5. Relationship between moisture content and cohesion for different soils

Table 5.4

	% < 2μ	dry density gr/cm³	author
1. Moraine	< 1	2.1	Bishop 1957
2. Moraine	2	1.93	"
3. Boulder clay	4	2.17	"
4. Boulder clay	10	2.1	"
5. Boulder clay	19	2.02	"
6. Sandy loam	±15	-	Bekker 1969
7. Lean clay	23	1.36-1.48	W.E.S. 1964
8. Residual clay	25	1.16	Bishop 1957
9. Clayey loam	35	-	Bekker 1969
10. Residual clay	44	1.54	Bishop 1957
11. Heavy clay	47	1.16-1.30	W.E.S. 1964

5.2.2. Cohesion and soil density

There is no substential influence of the soil density on the cohesion (see fig. 5.6 and table 5.5).

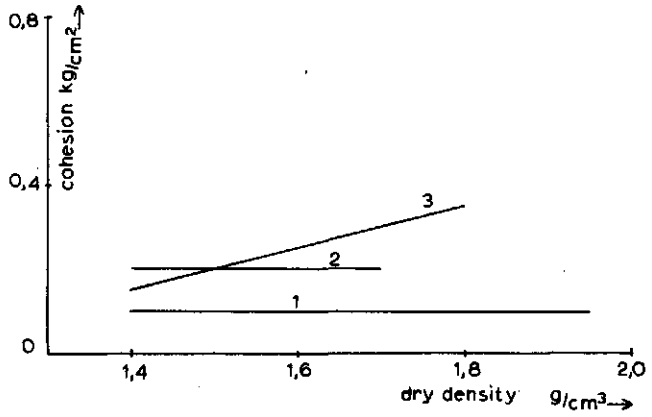

Fig. 5.6. Relation between soil density and cohesion for different soils

Table 5.5. Origin of the data from fig. 5.6.

	% < 2μ	author
1. Silt loam	5-18	Heidemij 1976
2. Loam	18-25	"
3. Sandy clay loam	25-35	"

5.3. S h e a r s t r e n g t h o f c o h e s i v e s o i l s

5.3.1. Difference between peak strength and ultimate strength

Fig. 5.7 indicates the stress-strain behavior of a hypothetical soil when carried well past the peak of the stress-strain curve. This picture has been pieced together from the observed behavior of a number of actuals soils. Some of the main features of this picture are.

1. The postpeak drop off in strength becomes more pronounced as the degree of overconsolidation increases, but can be quite noticeable even for normally consolidated soils.

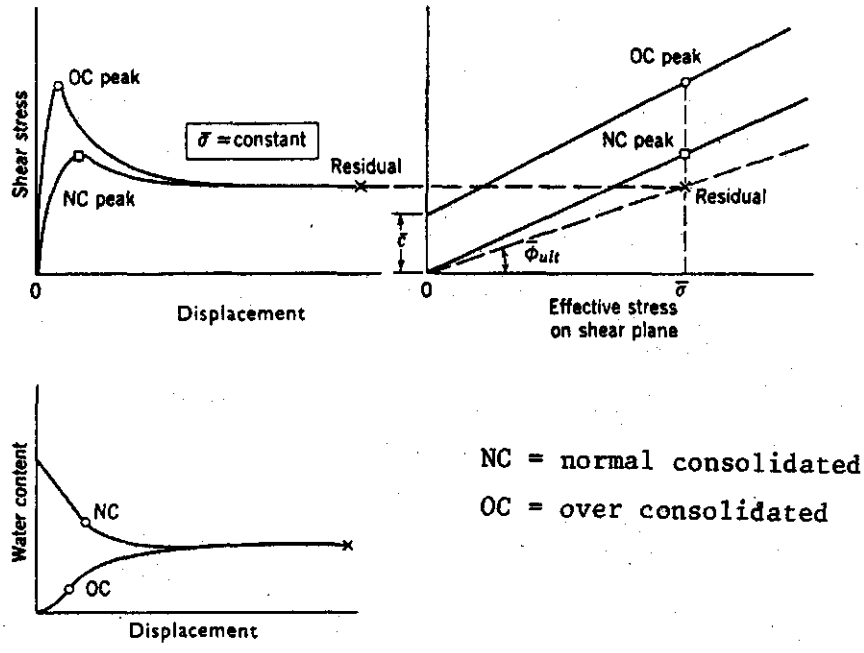

Fig. 5.7. Relationship between peak and ultimate conditions.
From LAMBE, 1969

2. In the ultimate condition the strength at a given effective stress is independent of past stress history. In fact, the ultimate strength of remolded and undisturbed specimens of a given soil have proved to be essentially the same.
3. The strength envelope for the ultimate condition is a straight line through the origin, generally at a position lower than that for the peak strength of the normally consolidated clay.
4. In the ultimate condition the water content for a given effective stress appears to be independent of past stress history. Actually it is very difficult to establish this as fact, because the failure zone tends to be very thin (perhaps only a few microns in thickness) and the water content of a slice cut from the clay may not be representative of the water content in the actual failure rate.

Thus the overall behavior of clay is essentially the same as that of sand: there is an ultimate condition wherein the strength and void ratio are independent of past history. In this ultimate condition, there really is a unique relationship among strength, effective stress

and density of packing.

However, there is one important difference between the ultimate strength behavior of sands and clays: in clays the ultimate strength can be significantly less than the peak strength of normally consolidated specimens, whereas the peak and ultimate resistance of loose sand are equal.

Although the progressive breaking of adhesive bonds may play a role in the postpeak drop off of the strength of normally consolidated clays a second factor that would seem to be even more important is the quadral reorientation of clay particles into parallel, face-to-face arrangements.

Such reorientation should be accompanied by a decrease in $\phi\mu$ and also a decrease in the degree of interlocking. This reorientation also seems to play a role with regard to the postpeak loss of strength in overconsolidated clays, in as much as some of this loss seems to occur after the clay has reached essentially constant volume.

There is good evidence that this reorientation occurs. Polished, slickensided surfaces have been found in direct shear tests after considerable strain.

Examination of failure zones using the electron microscope and X-ray techniques has indicated a highly orientated fabric. Finally it has been observed that the strength of clays at large strains decreases while the void ratio apparently is decreasing slightly, a phenomenon which can most readily be explained by reorientation.

5.3.2. Peak strength and ultimate strength for soils with different clay content

Fig. 5.8 indicates the way in which the ultimate friction angle varies with clay content. For clay contents approaching 100% the ultimate friction angles are of the same magnitude as $\phi\mu$ for the sheet minerals ($\phi\mu$ = interparticle friction). For very low clay contents ϕ ult. is of the same magnitude as $\phi\mu$ between quartz particles. In the general case, where the soil consists of both plate-like and granular particles, the granular particles tend to raise ϕ ult. above $\phi\mu$ for the clay particles by inhibiting to some extent the full orientation of the clay particles and by contributing some

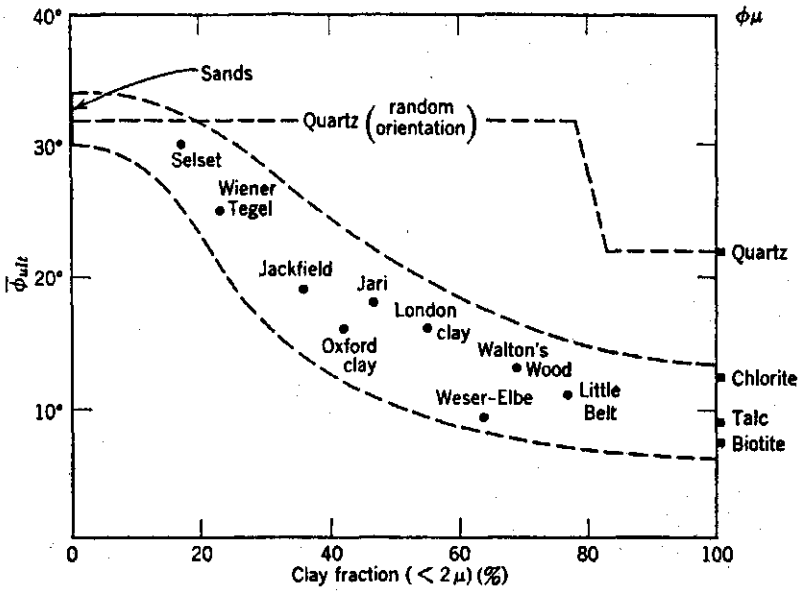

Fig. 5.8. Relations between $\bar{\phi}_{ult}$ and clay content (From SKEMPTON, 1964). From LAMBE, 1969

measure of their own higher angle of shear resistance. It is significant that the difference between $\bar{\phi}$ ult and $\bar{\phi}$ for normally consolidated soil also increases with increasing clay content.

This again indicates that reorientation of clay particles plays a major role in the drop off in strength past the peak of the stress-strain curve.

KOENIGS (1975) found for different saturated dutch marine clays substantial heigher values for ϕ (see fig. 5.9). ϕ was measured with a Torvane apparatus.

As in many other publications no distinction between peak and ultimate shear strength (or internal friction angle) was made.

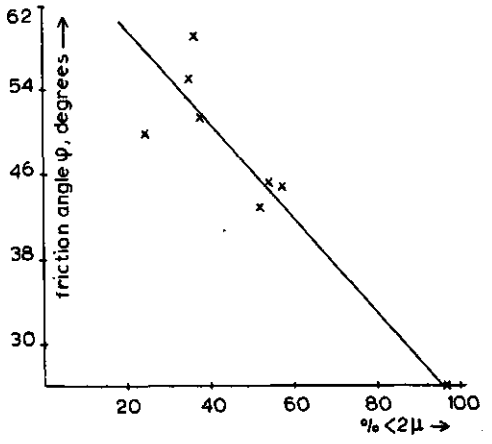

Fig. 5.9. Influence of clay content on the friction angle.
From KOENIGS, 1975

5.3.3. Effect of soil moisture content on the shear strength

VENEMAN (1976) found the relationship between soil moisture and shear strength (see fig. 5.10 and 5.11)

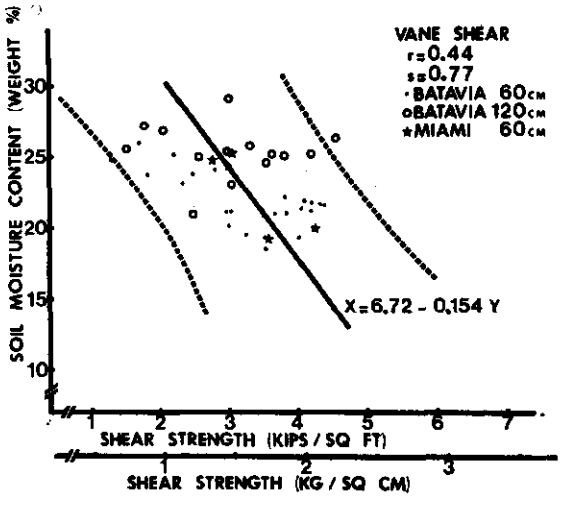

Fig. 5.10. Soil shear strength as measured with the vane shear test as a function of the soil moisture content (weight %).
Fron VENEMAN, 1976

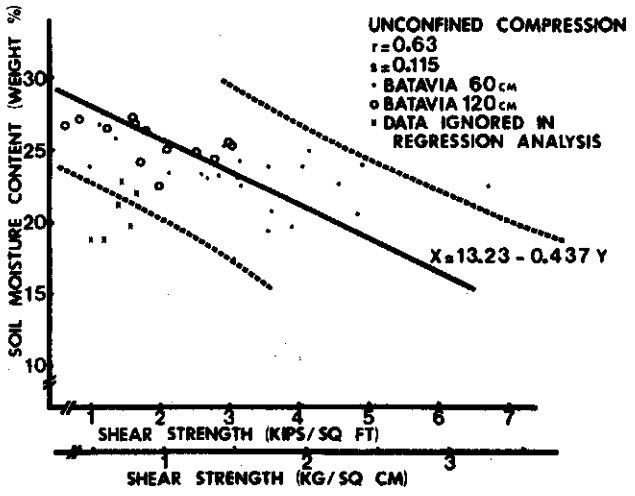

Fig. 5.11. Soil shear strength as measured with the unconfined compression test as a function of the soil moisture content (weight %). From VENEMAN, 1976

The soil tested was a silty clay loam (LL < 50%). They found a multiple regression equation for the shear strength as measured in-situ with the vane shear apparatus.

$$X = -3.84 - 0.18\,\theta w + 0{,}47U - 0{,}4PI$$

where

X = in-situ shear strength ($Kips/ft^2$)

θw = moisture content (weight %)

LL = liquid limit (%)

PI = plasticity index (%)

Inclusion of bulk density and clay content in the equation improved the correlation coefficient with only a factor of 0.029 which can be neglected.

POTAPOV (1966) found the following results from measurements with a Tolstoy apparatus with soil sample of 40 x 60 x 5-7 mm. The soil tested was a Sod-Podzolic (fine clay loam) - devided into two parts (47,95% < 0,01 mm - 12,8% < 0,001 mm)

I macrostructural samples - fractions 1-2 mm and < 25 mm

II microstructural samples - < 1 mm (for results see fig. 5.12)

and a chernozem (fine clay loam, 71,76% < 0,01 mm and 43,73% < 0,001 mm) (see fig. 5.13)

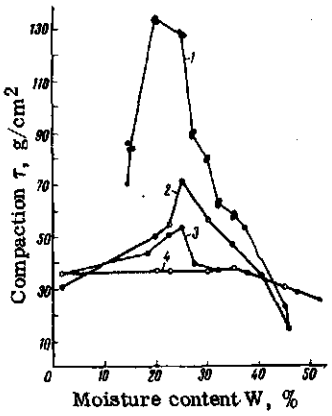

Fig. 5.12. Change in the maximum shear strength of samples of Sod-Podzolic soil as a function of moisture content. Microstructural samples: 1) during drying process; 2) during wetting process. Macrostructural samples: 3) during drying process; 4) during wetting process. From POTAPOV, 1966

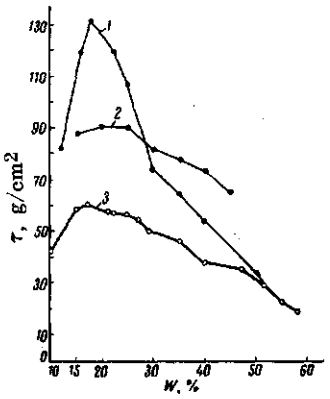

Fig. 5.13. Change in the maximum strength of microstructural samples of Chernozem soil as a function of the moisture content. 1) during drying process; 2) during mechanical compaction after wetting; 3) during wetting without additional compaction. From POTAPOV, 1966

He ran two series, one in which the samples were wetted to a moisture weight of 17,5-57,0% and one in which the samples were first wetted and then dried at 25°C to the desired moisture content.

Whenever microstructural samples are dried to a moisture content of 17% or less we see a decrease in the maximum shear strength as the result of the appearance of microtracks, which are noticeable in a twofold magnification.

For the Sod-Podzolic the compaction of the macrostructural samples vary between 0.82 and 0.85 g/cm^3, the compaction of the microstructural samples vary between 0.98 and 1.06 g/cm^3 under a load during the wetting process, but between 1.06 and 1.21 g/cm^3 during the drying process.

Compaction during drying gave a higher shear strength than mechanical compaction to the same density. Compaction during drying of chernozem soil varied between 1.01 and 1.14 g/cm^3 while the mechanical compaction was stopped at a density of 1.10 g/cm^3.

5.3.4. Physiochemical effects on the shear strength of clays

OLSON (1974) studied the influence of ion concentration on the shear strength of kaolinite, illite and montmorillonite.

The terms "physical" and "chemical" may be applied rather loosely to describe the interaction of particles. The term "physical" is used to denote interactions that are controlled largely by the size, shape, packing and physical properties of the individual grains and to the friction between them, whereas the term "chemical" is applied to interactions through diffuse double layers, van den Waals forces, and ionic forces.

For the three clay minerals studied the shearing strength appeared to be controlled mainly by the physical effects. No diffuse double layer effects were apparent for any of the clays in the calcium form.

For clays in the sodium form no diffuse double layer effect was noted for sodium illite.

For sodium montmorillonite the strengths were so low that reductions in normal effective stresses of 50% or more would probably go undetected.

Taken collectively the data suggest that location of the effective-stress failure envelope is controlled mainly by physical effects controlled by the size and shape of the individual particles.

Particles that are large and more or less equidimensional lead to high strengths regardless of chemical effects, whereas particles that are very thin with high diameter-to-thickness ratios, as in sodium montmorillonite, have very low strengths.

The values of $\bar{\phi}R$ were similar to the residual values of ϕ reported by Kenney (see OLSON, 1974). For a summary of the test results see fig. 5.14 where $\bar{R}$ denotes consolidated-undrained test and S consolidated-drained test.

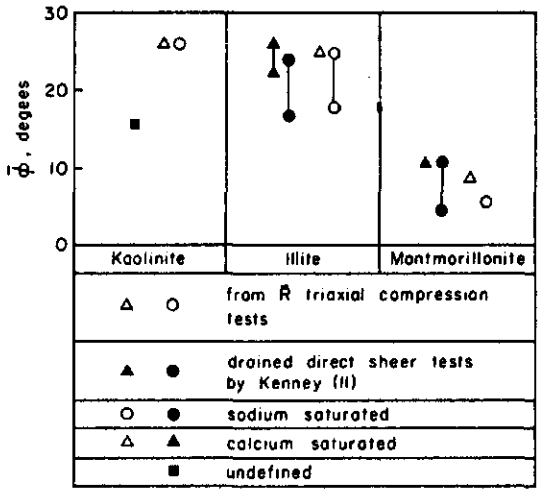

Fig. 5.14. Comparison of friction angles measured using $\bar{R}$ triaxial compression tests with residual angles measured using S direct shear tests on thin samples. From OLSON (1974)

The soil under investigation had following properties (table 5.6).

Table 5.6. Soil properties. From OLSON, 1974

Mineral (1)	Supplier, source, and trade name (2)	W_L, as a percentage (3)	W_P, as a percentage (4)	G, (5)	S, square meters per gram (6)	CEC, in milliequivalents per 100 g (7)	Finer than 2μ, as a percentage (8)	Estimated diameter height ratio (9)
Kaolinite	Minerals and Chemicals Philip Corp., McIntyre, Georgia, Klondyke Clay	40-50	27-31	2.65	14	1.5-4.5	47	2-5
Illite	Fithian, Illinois	65-90	35-40	2.85	90-100	25	100	10-50
Montmorillonite	American Colloids Co., Wyoming, Volclay	190-1,160	31-47	2.65-2.80	500-700	100	97	150-500

where W_L = liquid limit

W_P = plastic limit

G = density gr/cm^3

5.3.5. Influence of strain rate and confining pressure on the shear strength of compacted silt

Recent studies show that strain rate had little influence on the shear strength of cohesionless soils and a great influence on the shear strength of cohesive soils under undrained conditions (ROY, 1976, fig. 5.15). The strength of cohesive soils is considerably increased under very rapid rates of loading.

In fact it is necessary to settle the question of a suitable rate of axial strain for each specific soil.

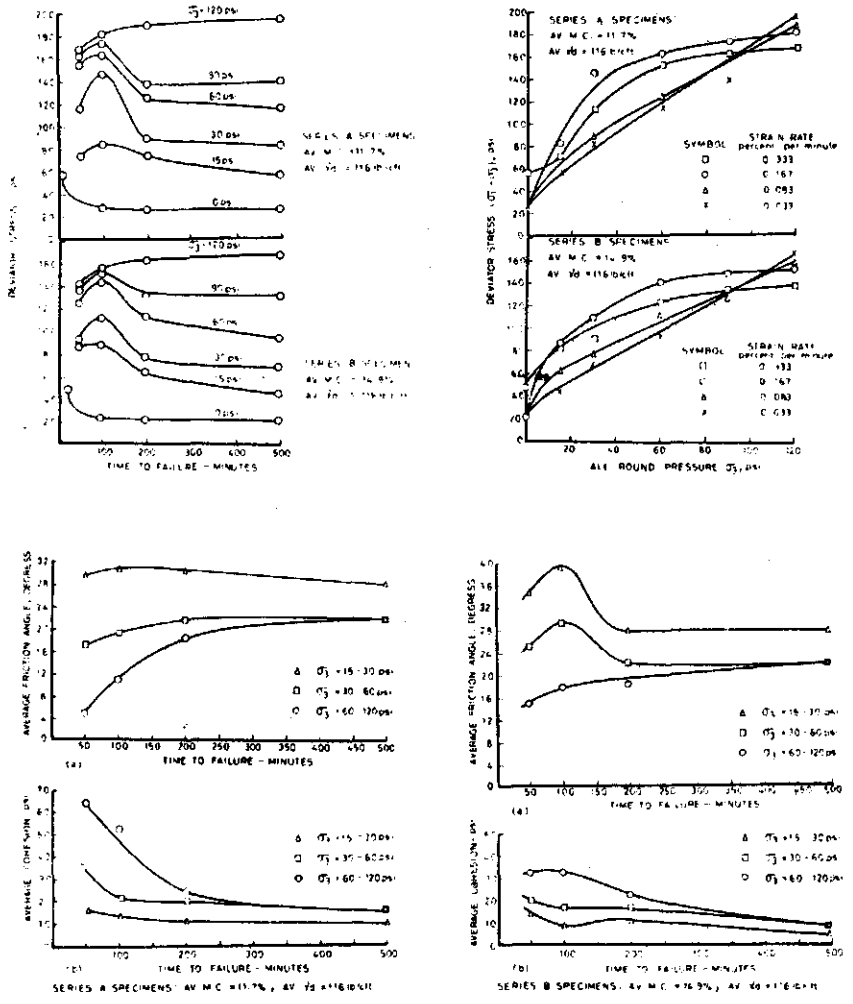

Fig. 5.15. Test results of triaxial tests under drained conditions and different confining pressures and loading rates. From ROY, 1976

Table 5.7. Characteristics of soils tested

	silt	fine sand	< 2μ
silty soil	85 %	10 %	5 %

mean particle size 0,01 mm
liquid limit = 34,6 %
plastic limit = 17,6 %
specific gravity = 2.67
Samples were compacted, following Standard Proctor test procedure at a dry density of 1860 kg/cm^3.

The fig. 5.15 (6 en 7) shows that cohesion decreases and angles of internal friction increases with decreasing confining pressure.

For the soil drier than the optimum the same trend also persists with increasing test duration and the rate of change in c and ϕ goes on decreasing with decreasing cell pressure until at a confining pressure range of (103,5 kN/m^2 - 207 kN/m^2) the shear strength parameters are practically uneffected by the speed of shear; c and ϕ remain virtually constant beyond the test duration of 200 min. at this pressure range. For soil wetter than the optimum the degree of saturation is high and at lower confining pressures (103,5 - 414 kN/m^2) range drainage appears to be poor at the faster rates of strain in variation of c and ϕ with speed erratic. For higher confining pressures the failure zone of the samples probably becomes fully saturated and with increasing test duration c and ϕ approach their drained values in a systematic manner.

For failure times greater than 200 min. variations in the values of c and ϕ with increasing failure time are similar for soils both drier and wetter than optimum. The 500 min. tests appear to be fully drained, i.e. at failure the shear parameters tend to reach identical values irrespective of whether the samples were initially drier or wetter than optimum.

5.3.6. Hyperbolic function to describe the stress-strain relation of compacted clays

DANIEL and OLSON (1974) found that the hyperbolic curve originally

used by Kondner fit the data of the triaxial stress-strain curve better than any other simple expression.

Kondner's expression is of the form

$$\sigma 1-\sigma 3 = \frac{\varepsilon a}{a + b\,\varepsilon a} \qquad (1)$$

where $\sigma 1-\sigma 3$ = stress difference

εa = axial strain

a and b = constants.

The constants a and b can be found by rearranging eq. 1 to

$$\frac{\varepsilon a}{\sigma 1-\sigma 3} = a + b\varepsilon a \qquad (2)$$

and then plotting $\varepsilon a/\sigma 1-\sigma 3$ versus εa. If the hyperbola (1) describes the stress-strain curve accurately, then the experimental data should all plot on a single straight line in the transformed plot with intercept a and slope b.

Another method for finding a and b is to fit the hyberbola through two points on the stress-strain curve where the stress difference is equal to 70% and 95% of the peak stress difference.

Physical significance of Kondner's constants.
Kondner demonstrated that constants a and b have a physical meaning, i.e. a is the reciprocal of the initial largest modulus and b is the stress difference to which the hyperbola becomes asymptotic at infinite strain. Kondner noted that the experimental stress difference at failure is somewhat less than the stress difference to which the hyperbola becomes asymptotic and presented the following hyperbolic equation

$$\sigma 1-\sigma 3 = \frac{Ea}{\frac{1}{E_i} + \frac{Rf}{(\sigma 1-\sigma 3)f}\,Ea} \qquad (3)$$

where

E_i = initial tangent modulus

$(\sigma 1-\sigma 3)f$ = the experimental stress difference at failure

Rf = failure ratio which is defined as the ratio of the experimental stress difference at failure to the reciprocal of Kondner's constant b.

Influence of confining pressure.

To use eq. 3 to approximate the stress-strain curves of compacted soils it is necessary to express Ei, (σ1-σ3)f and Rf as analytical functions of such independent variables as compaction water content and confining pressure, with soil type and compaction procedure held constant.

Correlation of Ei with confining pressure.

Janbu developed the following equation for the relationship between EI and σ3: see DANIEL (1974)

$$\frac{Ei}{Pa} = K \left(\frac{\sigma 3}{Pa}\right)^n \qquad (4)$$

in which Pa = the atmospheric pressure expressed in the same units as σ3 and Ei; and K and n are dimensionless constants. The equation is in such a form that a plot of log Ei/Pa versus log (σ3/Pa) for the experimental data should define a straight line.

A typical plot of log (Ei/Pa) versus log (σ3/Pa) is presented in fig. 5.16 for a wide range in compaction water contents.

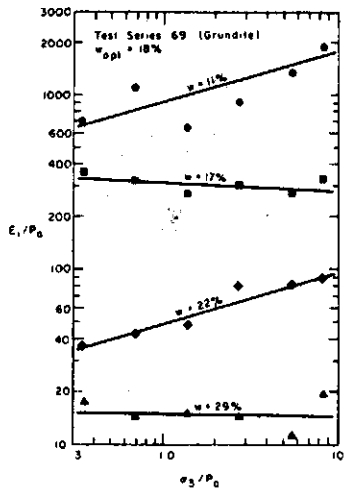

Fig. 5.16. Log Ei/Pa versus log (σ3/Pa) for a wide range of compaction water contents.
From DANIEL (1974)

Eq. 4 apparently accounts for the variation of Ei with confining pressure and compaction water content with reasonable accuracy. Note that Ei in fig. 5.16 is the reciproval of Kondner's a coefficient, not an Ei measured from the experimental curves. The values of K and n may readily be evaluated from plots such as fig. 5.16. The value of K is numerically equal to the value of Ei/Pa when $\sigma 3/Pa=1$ and n is the slope of the line of best fit.

Correlation of stress difference at failure with confining pressure.

For confining pressures smaller than about 100 psi (7 kg/m^2) $(\sigma 1-\sigma 3)f$ is approximately a linear function of the confining pressure fig. 5.17 and the strength may be expressed by

$$(\sigma 1-\sigma 3)f = d + \sigma 3 \tan \phi \qquad (5)$$

in which d = the intercept; and ϕ = the slope of the failure envelope.

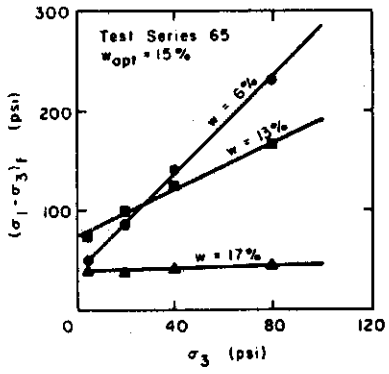

Fig. 5.17. Failure envelopes for confining pressures smaller than 100 psi (1 psi = 6.89 kN/m^2). From DANIEL, 1974

The slope of the failure envelope usually decreases as the compaction water content increases (fig. 5.17), but the intercept has a maximum at a water content just dry of the optimum water content (fig. 5.18).

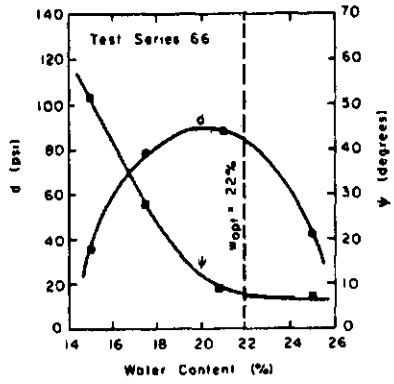

Fig. 5.18. Shear strength parameters for compacted clay as functions of compaction water content (1 psi = 6.89 kN/m^2). From DANIEL, 1974

For confining pressures above 100 psi (7 kg/cm^2) it is usually more accurate to assume a linear relationship between log ($\sigma 1-\sigma 3$) and log $\sigma 3$ (fig. 5.19) and to use the following relationship

$$(\sigma 1-\sigma 3)f = K\sigma 3^{\tan \phi} \qquad (6)$$

in which K is numerically equal to the value of ($\sigma 1-\sigma 3$)f when $\sigma 3=1$; and ϕ = the slope of the failure envelope in the log-log diagram.

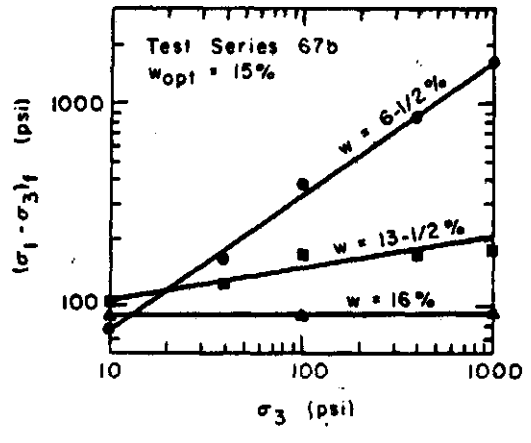

Fig. 5.19. Failure envelopes for confining pressures up to 1,000 psi (1 psi = 6.89 kN/m^2). From DANIEL, 1974

DANIEL (1974) supports the recommandation of Hunter and Chang that Rf can be teken as a constant equal to 0.9.

So the stress-dependent hyperbolic equation may now be written as follows

$$\sigma 1-\sigma 3 = \frac{Ea}{\frac{1}{KPa\left(\frac{\sigma 3}{Pa}\right)^n} + \frac{0.90}{d + \sigma 3 \tan\phi}} \qquad (7)$$

for the case of a linear failure envelope.

Fig. 5.20 shows some examples of fitting the hyperbola to the experimental data.

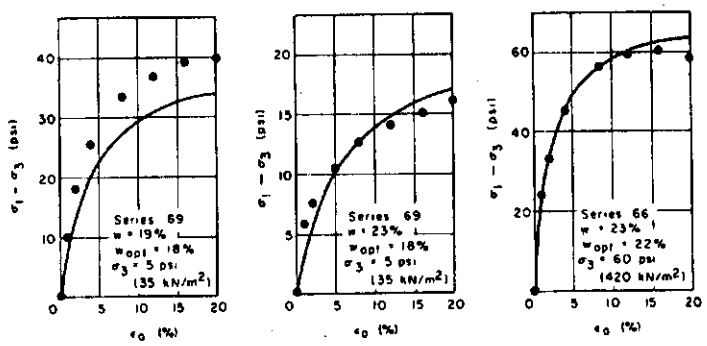

Fig. 5.20. Examples of 'poor', 'average', and 'good' correlations between theoretical and experimental stress-strain curves (1 psi = 6.89 kN/m^2).
From DANIEL, 1974

The test procedure used here was the unconsolidated-undrained triaxial test on homogeneous and isotropic compacted specimens.

DANIEL (1974) describes also analytic expressions for Poisson's ratio, i.e. the influence of axial strain and confining pressure on Poisson's ratio.

5.3.7. Effect of consolidation on the drained shear strength of clays

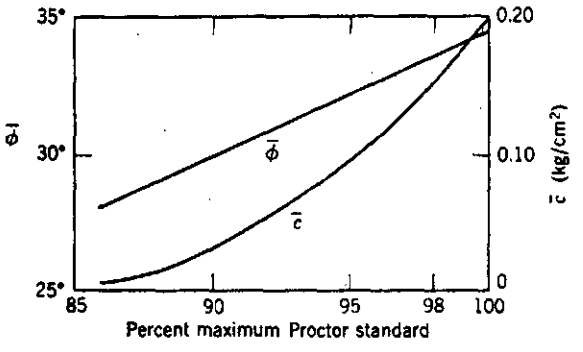

$\bar{c}$ = cohesion intercept based on effective stress concept

$\bar{\phi}$ = angle of internal friction based on effective stress concept

Fig. 5.21. Effect of compactive effort on strength parameters of clayey sand (after MORETTO ET AL., 1973). From LAMBE, 1969

Typical Values of $\bar{c}$ and $\bar{\phi}$ for Overconsolidated Clays. From LAMBE and WHITMAN, 1969

The magnitude of $\bar{c}$ and $\bar{\phi}$ for a given clay depends on how large the preconsolidation stress has been, how long the clay has been under the preconsolidation stress, etc. The effect of preconsilidation can best be illustrated by data for a compacted soil (fig. 5.21), where the compactive effort supplies the preconsilidation.

The $\bar{c}$ and $\bar{\phi}$ for a given soil also depend on the stress range over which a straight line fit is made to the curved Mohr envelope: Thus

1. When effective stress is a large fraction of preconsolidation stress, ϕ will be slightly less than for normally consolidated clay, while $\bar{c}$ will depend on the magnitude of preconsolidation stress (void ratio).
2. When effective stress is very small compared to preconsolidation stress, $\bar{c}$ will be relatively small and ϕ will depend on magnitude of preconsolidation stress (void ratio).

Fig. 5.22 illustrates (to an extreme degree) the way in which $\bar{c}$ and $\bar{\phi}$ can vary with the stress range. The Mohr envelope for an overconsolidated soil seldom is as that in fig. 5.22.

Usually the ϕ from a straight-line fit to an overconsolidated clay is about equal to that for normally consolidated specimens. Moreover, the effects of preconsolidation on strength are important numerically only at small effective stresses; at large effective stresses the envelopes for normally and overconsolidated specimens of a clay tend to merge. Thus the major question with regard to overconsolidated clay lies in choosing the appropriate value of $\bar{c}$. Values of $\bar{c}$ ranging from 0,05 - 0,25 kg/cm^2 are often used for soils. Even larger values undoubtedly are valid for the stiffest of soils, but large "measured" $\bar{c}$ values frequently result from running CD tests too rapidly so that pore pressures develop. Extreme caution must be exercised when choosing a value of $\bar{c}$ for practical calculations.

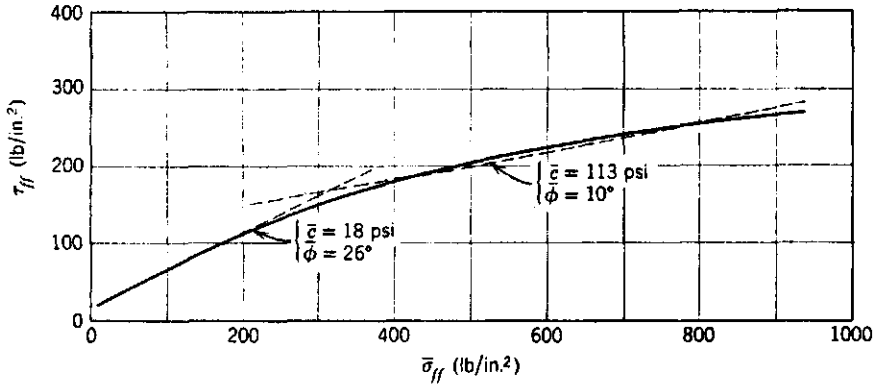

Fig. 5.22. Strength evenlope for unweathered London clay (from BISHIP, ET AL., 1965).
From LAMBE, 1969

5.3.8. Influence of soil density on the shear strength

ANDERSON (1976) gave the values shown in fig. 5.23 for the shear strength of soils with different density.

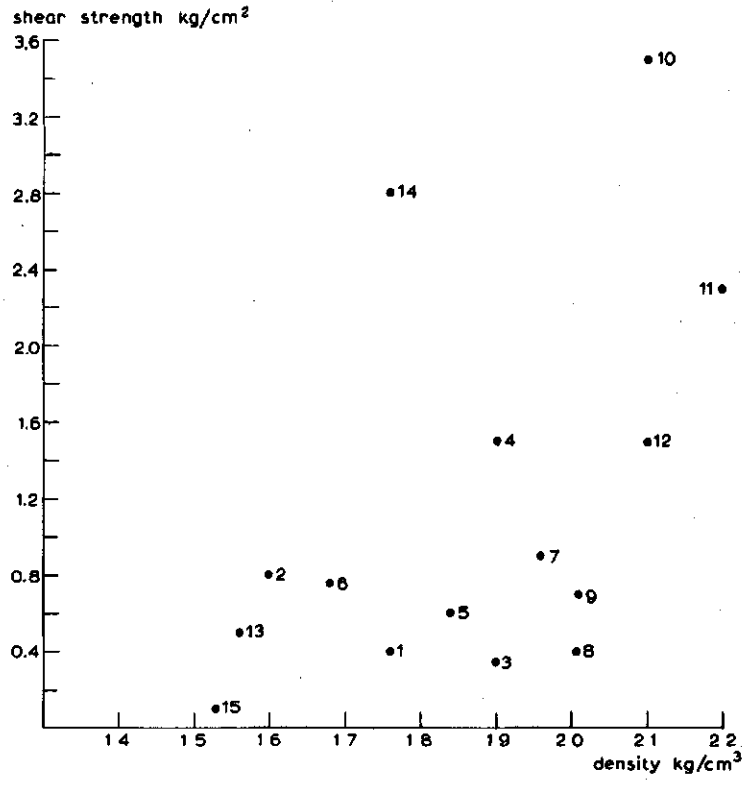

Fig. 5.23. Relation between shear strength and density.
From ANDERSON, 1976

The data are taken from table 5.7. There seems to be a relation between density and shear strength. Due to the different test methods used in table 5.7 it is very dangerous to establish relationships between shear strength and other soil parameters such as clay content, soil density, etc. from these data.

Table 5.7. from ANDERSON, 1976

Soil name (1)	Sample depth, in feet (2)	Test number (3)	e_o (4)	γ, in pounds per cubic feet (5)	gr. per cm^3	G_s (6)	S_l, as a percentage (7)	W_{ll}, as a percentage (8)	I_p, as a percentage (9)	D_{50}, in millimeters (10)	Percentage less than 2μ (11)	P_c, in kg per cm^3 (12)	Undrained Shearing Strength* S_u, in kg per cm^3 (13)	Test method (14)
Ball	–	K3	1.11	110	1.76	2.65	97	71	39	0.00025	84 (1)**	1.4	0.4	UC
Kaolinite	–	K4	1.09	111	1.77	–	97	–	–	–	–	–	–	–
Bentonite-Silica	–	BS1	1.88	99	1.58	–	100	–	–	–	–	–	–	–
	–	BS2	1.87	100	1.60	2.70	100	96	64	0.003	47 (2)	<0.2	0.8	VS
	–	BS3	2.01	97	1.55	–	100	–	–	–	–	–	–	–
Detroit clay	10	R2-1	0.89	120	1.9	–	100	30	12	0.002	49 (3)	1.0	0.35	–
	14	R3-3	0.82	119	1.9	–	92	36	15	0.002	51 (4)	1.9	1.5	–
	26	R3-8a	1.24	109	1.75	–	98	44	20	0.009	26	–	–	–
	26	R3-8b	1.09	115	1.84	–	100	–	–	–	– (5)	–	≈0.6	VS and UC
	32.5	R3-11a	1.45	105	1.68	–	97	55	30	0.04	12 (6)	2.0	0.4	–
Ford clay	–	F1	0.88	117	1.27	–	94	–	–	–	–	–	–	–
Eaton clay	≈6	F2	0.75	123	1,96	2.71	100	37	19	0.0035	42 (7)	3.3	0.9	CU
Chevy clay	14	E1	0.62	128	2.04	–	100	35	17	0.004	40 (8)	1.7	0.4	–
	20	E2	0.70	126	2.08	–	100	40	20	0.002	50 (9)	2.2	0.7	UC
	21	C3	0.46	132	2.1	–	81	25	10	0.01	27 (10)	–	3.5	–
	35	C1	0.41	138	2.2	2.71	100	–	–	0.01	27 (11)	>10.0	2.3	UC
	35	C2	0.39	138	2.2	–	100	–	–	–	–	–	–	–
	51	C4	0.50	131	2.1	–	86	25	10	0.018	20 (12)	–	1.5	–
Leda clay I	15.5	L4a	2.14	97	1.55	–	97	69	44	0.0005	78	–	–	–
	15.5	L4b	2.04	98	1.56	2.74	98	–	–	–	– (13)	2.2	0.5	UC and CU
	16	L3	2.18	95	1.52	–	96	–	–	–	–	–	–	–
	17	L2	2.05	96	1.53	–	97	67	37	–	–	–	–	–
Leda clay II	–	LB1	1.13	110	1.76	2.74	93	–	–	0.0015	55 (14)	3.2	2.8	UC
	–	LB2	1.12	112	1.79	–	95	–	–	–	–	–	–	–
Gulf of Mexico clay	22	M1	2.13	96	1.53	2.70	100	89	54	0.0011	55 (15)	–	0.1	VS
	25	M2	1.98	97	1.53	–	97	85	50	–	–	–	–	–
Santa Barbara clay	–	–	–	–	–	–	–	–	–	–	–	–	–	–
	25	A1	2.28	–	–	2.72	96	83	44	–	–	0.46	0.2	CU
Ostiglia clay	16.4	11	0.69	125	2.0	–	98	–	–	0.040	13	–	–	–
	16.5	12	0.77	122	1.95	–	99	–	–	0.026	14	–	–	–
	23	13	0.74	123	1.96	–	98	–	–	0.024	16	–	–	–

*Data from unconfined compression tests ((C), vane shear tests (VS), consolidated (at estimated in-situ overburden pressure) undrained triaxial tests (CU). Note: 1 ft = 0.305 m; 1 pcf = 16,01 kg/m^3

**Data used in fig. 5.23

5.3.9. Values of the c and ϕ (from undrained consolidated triaxial tests)

Soil	clay content	dry density gr/cm^3	water content % dry weight	cohesion kg/cm^2 c	friction angle degrees ϕ
Moraine	< 1	2.1	6.8	0.43	42
			8.8	0.37	44
			10.2	0.056	41
Moraine	2	1.93	9.6	0.7	36
			12.2	0.48	37
			14.8	0.0	36
Boulder clay	4	2.17	6.8	0.64	38
			7.8	0.48	38
			8.8	0.13	37
Boulder clay	10	2.1	9.5	0.7	33
Sandy loam	10	-	12	0.07	32
			16	0.14	28
			20	0.12	24
			24	0.07	18
Boulder clay	19	2.02	8.8	1.15	27
			10.7	0.81	24
			12.4	0.24	28
Lean Clay	23	1.48	22	0.49	18
		1.50	26	0.42	6
		1.41	30	0.26	0
		1.36	32	0.14	0
Residual clay	25	1.16	48.2	0.59	31
Clayey clay	28-40	-	38	0.035	14
			42	0.053	15
			46	0.059	16
			51	0.039	10
Residual clay	44	1.54	20	1.27	24
			23	1.103	21
			25	0.30	24
Heavy clay	47	1.30	25	0.50	12
		1.32	35	0.30	1
		1.22	40	0.16	0
		1.16	45	0.10	0

LITERATURE FRICTION ANGLE, COHESION AND SHEAR STRENGTH CHAPTER 5.
OF COHESIVE SOILS.

ANDERSON, DONALD G. and RICHARD D. WOODS. Time-Dependent Increase in Shear modulus of clay. Journal of the Geotechnical Engineering division. No. 5 - 1976, p. 525-537.

BEKKER, M.G. Introduction to Terrain-Vehicle Systems. University of Michegan Press, Ann Arbor 1969

BISHOP, ALAN W. and D.J. HENKEL, 1957. The measurement of soil properties in the triaxial test. Edward Arnold (Publishers) L.T.D. London.

DANIEL, David E. and ROY E. OLSON. Stress-Strain Properties of Compacted Clays. Journal of the Geotechnical Engineering Division, no. 10 - october 1974.

HEIDEMIJ. Bodemkundig-Grondmechanisch rapport. Rapport nr. 667-76/3. Hoofdwatergangen in de ruilverkaveling Voorne-Putten. Dienst voor de landinrichting in Zuid-Holland.

HUMPHREYS, J.D. Some empirical relationships between drained friction angles, mechanical analyses and Atterberg limits of natural soils at Kainji Dam, Nigeria. Geotechnique, vol. 25, no. 3 - sept. 1975.

KAINJI. The relationship between drained friction angles and Attenberg limits of natural soils. Geotechnique, vol. 24, no. 4 - dec. 1974, pp. 671-674.

KOENIGS, F.F.R. Apparent volume and shear strength of consolidated submerged sediments. Geotechnique 25, no. 2, pp. 265-278.

LAMBE, T. WILLIAM and ROBERT V. WHITMAN. Soil Mechanics Massaschusetts Institute of Technology, 1969. John Wiley and Sons, Inc., New York.

MIRATA, T. The in-situ wedge shear test - a new technique in soil density. Geotechnique 24, no 3, pp. 311-332.

OLSON, ROY, E. Shearing Strengths of Kaoline, Illite and Montmorillonite. Journal of the Geotechnical engineering division, no. 11 - november 1974.

POTAPOV, B.I. Influence of moisture content and soil compaction on the soil's maximum shear strength - Soviet Soil Science - april 1966, no. 4, page 396.

ROY NIKHILESH and PANTH SARATHI. Strain Rate Behavior of Compacted Silt. Geographical Vol. no. 4, april 1976, p. 347-360.

VENEMAN, P.L.M., J. BOUMA and T.B. EDIL. Soil shear strength variation in soils of a Bavaria Silt loam mapping unit. Soil Sci. Soc. Am. J. Vol. 40, 1976.

VOMOCIL, J.A. and W.J. CHANCELLOR, 1967. Compressive and Tensile Faiure Strengths of three agricultural soils. Transaction of ASCE 1967 Vol. 10, no. 4.

W.E.S. U.S. Army Engineering Waterways, Experiment Station Technical Report no. 3-639. Corps of engineers. Vicksburg, Mississipi, january 1964.